Institut für Veterinärphysiologie
der Vetsuisse-Fakultät Universität Zürich

Direktor: Prof. Dr. Max Gassmann

Arbeit unter Leitung von PD Dr. Thomas Riediger

Involvement of amylin and leptin in early developmental programming of brain pathways controlling energy balance and body weight

Inaugural-Dissertation

zur Erlangung der Doktorwürde der
Vetsuisse-Fakultät Universität Zürich

vorgelegt von

Kathrin Abegg

Tierärztin
von Horgen, Schweiz

genehmigt auf Antrag von
PD Dr. Thomas Riediger, Referent
Prof. Dr. Kurt Bürki, Korreferent

Zürich 2010

LIST OF ABBREVIATIONS III

SUMMARY IV

ZUSAMMENFASSUNG V

1 INTRODUCTION 1

1.1 Energy homeostasis 1

1.1.1 Satiation signals 1

1.1.2 Adiposity signals 2

1.2 Amylin 3

1.2.1 Structure, tissue expression and secretion 3

1.2.2 Influence on nutrient fluxes 3

1.2.3 Effects on food intake 4

1.2.4 Amylin and diabetes mellitus 4

1.3 Area postrema 5

1.3.1 Functions of the AP 6

1.4 The arcuate nucleus of the hypothalamus 8

1.5 Amylin knockout mice 9

1.6 Leptin-deficient ob/ob mice 10

1.6.1 Neurotrophic effects of leptin 10

1.7 Aim of the study 11

2 MATERIALS AND METHODS 13

2.1 Animals 13

2.1.1 Generation of amylin knockout mice 13

2.1.2 Animal breeding and housing 13

2.2 DiI fiber labeling 15

2.2.1 Perfusion and tissue fixation 15

2.2.2 DiI Implantation 17

2.2.3 Brain slicing 21

2.2.4 Fluorescence microscopy 22

2.2.5 Confocal laser microscopy 24
2.2.6 Quantitative analysis 25

2.3 Immunohistochemistry 25
2.3.1 Perfusion and tissue fixation 26
2.3.2 Brain slicing 26
2.3.3 Immunohistochemistry for c-Fos 27
2.3.4 Immunohistochemistry for calcitonin receptors 28

2.4 Genotyping 30
2.4.1 DNA extraction 30
2.4.2 DNA amplification 32
2.4.3 DNA separation 34

2.5 Statistical analysis 36

3 RESULTS 37

3.1 Neurotrophic effects of amylin 37
3.1.1 Fiber density in the NTS on P10, P14 and P60 37

3.2 c-Fos expression and calcitonin receptor density in the AP 42
3.2.1 c-Fos expression in the AP/NTS region of adult mice 42
3.2.2 Calcitonin receptor density in the AP of adult mice 44

3.3 Neurotrophic effects of leptin in the AP 46
3.3.1 Fiber density in the NTS on P14 46
3.3.2 Long projections to other brain regions 47

3.4 Establishment of ARH implantations 49

4 DISCUSSION 52

5 REFERENCES 58

6 ACKNOWLEDGEMENT 69

LIST OF ABBREVIATIONS

α-MSH	α-melanocyte stimulating hormone
AgRP	agouti-related protein
AM	adrenomedullin
ANGII	angiotensin II
AP	area postrema
ARH	arcuate nucleus of the hypothalamus
AVP	arginine vasopressin
BNST	bed nucleus of the stria terminalis
CCK	cholecystokinin
CeA	central nucleus of the amygdala
CNS	central nervous system
CT	calcitonin
CTA	conditioned taste aversion
CVO	circumventricular organs
db/db mouse	leptin receptor deficient mouse
DMH	dorsomedial nucleus of the hypothalamus
GABA	gamma aminobutyric acid
het	heterozygous
IAPP	islet amyloid polypeptide
IVGTT	intravenous glucose tolerance test
ko	knock out
LHA	lateral hypothalamic area
NPY	neuropeptide Y
NTS	nucleus of the solitary tract
ob/ob mouse	leptin deficient mouse
OGTT	oral glucose tolerance test
OVLT	organum vasculosum of the lamina terminalis
(L)PBN	(lateral) parabrachial nucleus
POMC	pro-opiomelanocortin
PVH	paraventricular hypothalamic nucleus
RAMP	receptor activity modifying protein
RI1P-gIAPP	rat insulin-I promotor-human IAPP fusion gene
SFO	subfornical organ
T2DM	type 2 diabetes mellitus
wt	wildtype

SUMMARY

Amylin is a peptide hormone that is synthesized by pancreatic ß-cells and secreted in response to nutrient stimuli. It acts as a satiation signal, inhibiting food intake by limiting meal size. The adipocyte-derived hormone leptin exerts trophic effects on projections from its central site of action. In the current study, we investigated the neurotrophic effects of amylin and leptin on the development of projections from the area postrema (AP), amylin's central site of action, to the nucleus of the solitary tract (NTS) in mouse pups and possible functional consequences.

We implanted crystals of the lipophilic tracer DiI into the AP of male amylin-deficient $IAPP^{-/-}$ mice and their wildtype $IAPP^{+/+}$ littermates on postnatal day 10 (P10), 14 (P14) and 60 (P60), and of leptin-deficient *ob/ob* and wildtype (*wt*) littermates on P14, to label projections to the NTS.

In $IAPP^{+/+}$ mice, AP-NTS projection fiber density regressed from P10 to P14, indicating neuronal remodeling processes. There was no difference in fiber density or signal transduction between the two genotypes on P60. However, there were indications of compensatory receptor upregulation mechanisms in P60 $IAPP^{-/-}$ mice.

In *ob/ob* mice, AP-NTS fiber density was significantly reduced on P14 compared to *wt* littermates. Our findings extend the concept that amylin and leptin function as developmental factors in the maturation of brain circuits maintaining energy balance.

ZUSAMMENFASSUNG

Amylin ist ein Peptidhormon, welches nach Nahrungsaufnahme sezerniert wird und als Sättigungssignal wirkt. Das Hormon Leptin wird von weissen Fettzellen sezerniert und übt trophische Effekte auf neuronale Projektionen seiner zentralen Zielstruktur aus. Wir untersuchten die neurotrophe Wirkung von Amylin und Leptin auf die Entwicklung neuronaler Projektionen von der Area Postrema (AP), der zentralen Zielstruktur von Amylin, zum Nucleus tractus solitarii (NTS) bei Mäusewelpen, sowie mögliche funktionelle Folgen.

Wir implantierten Kristalle des lipophilen Fluoreszenzfarbstoffes DiI in die AP von Amylin-defizienten $IAPP^{-/-}$ Mäusen und Wildtyp $IAPP^{+/+}$ Wurfgeschwistern am postnatalen Tag 10 (P10), 14 und 60, und von Leptin-defizienten *ob/ob* und Wildtyp (*wt*) Wurfgeschwistern an P14, um Projektionen zum NTS zu quantifizieren

Die Dichte der AP-NTS Projektionsfasern von $IAPP^{+/+}$ Mäusen reduzierte sich zwischen P10 und P14, was auf neuronale Umgestaltung hinweist. An P60 konnte kein Unterschied in der Faserdichte oder der Signalübermittlung zwischen den Genotypen gefunden werden; es gab jedoch Hinweise auf eine kompensatorisch vermehrte Rezeptorexpression in P60 $IAPP^{-/-}$ Mäusen.

Die Faserdichte von *ob/ob* Mäusen an P14 war im Vergleich zu *wt* Wurfgeschwistern signifikant reduziert. Unsere Resultate erweitern das Konzept, dass Amylin und Leptin als Entwicklungsfaktoren bei der Reifung von neuronalen Schaltkreisen dienen, welche in die Aufrechterhaltung der Energiehomöostase involviert sind.

1 Introduction

1.1 Energy homeostasis

Maintenance of energy homeostasis, i.e. the balance between energy intake and energy expenditure, is crucial to keep body weight stable (Berridge 2004). The modern world is confronted with a wide increase in the prevalence of obesity (Popkin and Doak 1998) and of related disorders such as diabetes mellitus, atherosclerosis and hypertension; together, they express the dramatic consequences of imbalances in energy homeostasis (Molavi et al. 2006).

The hormonal system controlling energy intake consists of two main categories, satiation signals and adiposity signals, which are sensed and integrated by the central nervous system (CNS) (Luquet and Magnan 2009; Woods et al. 2004).

1.1.1 Satiation signals

It is widely accepted today that the main control of short term food intake and meal size in particular is not exerted at the time of meal onset but at meal termination; therefore, the amount of food consumed is controlled, thus allowing individuals flexibility and adaptation to their environment (Woods et al. 2000). This control depends on the exact measurement of amount and composition of the food already eaten, which is provided by hormonal and neuronal enteroceptive signals. Sham feeding studies have shown that those signals mainly arise from the distal stomach or small intestine, as animals with open gastric fistula consume significantly larger meals (Davis and Campbell 1973).

The first identified satiation signal was cholecystokinin (CCK). CCK dose-dependently reduces meal size in rats if administered prior to a meal (Gibbs et al. 1973). CCK is a peptide secreted by the duodenal and jejunal mucosa in response to luminal nutrients. It facilitates digestion by stimulating enzyme secretion of exocrine pancreas and liver, and by gallbladder contraction (Moriyasu et al. 1994). In addition, CCK's satiating effect is mediated by a stimulation of CCK receptors on sensory fibers of the vagus nerve that project to the nucleus of the solitary tract in the hindbrain (Moran et al. 1997), and possibly by receptors located in the hypothalamus (Blevins et al. 2000).

Similar to CCK many other gastrointestinal peptides are released in response to food intake and have been reported to inhibit feeding, such as peptide YY(3-36) (Batterham et al. 2002), gastrin releasing peptide (Stein and Woods 1982), glucagon-like peptide-1 (Naslund et al. 1999), neuromedin B (Ladenheim et al. 1996), apolipoprotein A-1V (Fujimoto et al. 1993),

somatostatin (Lotter et al. 1981) and enterostatin (Okada et al. 1991; Shargill et al. 1991). Furthermore, amylin (Lutz et al. 1994) and glucagon (Geary 1990), which are secreted from the pancreatic islets in response to food intake, also reduce meal size when administered peripherally before the meal. Except for CCK and probably amylin and glucagon, the physiological relevance of the eating inhibitory effects of these hormones still needs to be confirmed.

Most of those signals stimulate the hindbrain either directly at sites lacking a functional blood brain barrier, such as amylin in the area postrema (AP) (Lutz et al. 1995a), or by activating afferent vagal fibers projecting to the hindbrain, which are also activated by gastrointestinal mechano- and chemosensors (Anand and Pillai 1967).

1.1.2 Adiposity signals

Adiposity signals are hormones secreted in direct proportion to the amount of body fat. The best characterized are leptin, secreted directly from white adipocytes (Dua et al. 1996; Havel 1999; Maffei et al. 1995), and insulin, which is secreted from pancreatic beta cells (Bjorntorp 1997; Polonsky et al. 1988). Both can cross the blood-brain barrier by saturable transport (Banks et al. 1997; Banks et al. 1996) and are thought to act directly on the arcuate nucleus of the hypothalamus (ARH) by stimulating neurons containing pro-opiomelanocortin (POMC) and by inhibiting neurons containing agouti-related protein and neuropeptide Y (AgRP/NPY). POMC neurons release α-melanocyte stimulating hormone (αMSH), which exerts catabolic and anorexigenic actions. AgRP/NPY neurons release AgRP and NPY into the paraventricular nucleus of the hypothalamus; further, they release gamma aminobutyric acid (GABA) within the ARH, which acts anabolic and orexigenic mainly by inhibiting POMC neurons (Baskin et al. 1999; Benoit et al. 2002). In addition, insulin and leptin have both been shown to modulate the sensitivity to satiation signals. Hence, excessive weight gain, leading to increased plasma leptin and insulin levels, results in an increased sensitivity to the meal size reducing effects of CCK (Matson et al. 1997; Riedy et al. 1995).

Any disruption in leptin signaling results in severe weight gain, which is apparent in leptin deficient (*ob/ob*) and leptin receptor deficient (*db/db*) mice. (Friedman and Halaas 1998; Tartaglia 1997).

1.2 Amylin

1.2.1 Structure, tissue expression and secretion

Amylin is a 37–amino-acid peptide that was first isolated from amyloid-containing pancreata of humans with type 2 diabetes (Clark et al. 1987; Cooper et al. 1987). Because of its origin, the isolated peptide was first named “diabetes-associated peptide” or “islet amyloid polypeptide” (IAPP), but was renamed to amylin after the discovery that it was also present under non-pathologic conditions (Cooper et al. 1988), acting as a hormone. Today, amylin is the most commonly used term, but the term IAPP, designated 1987 by *Westermark* (Westermark et al. 1987), is often used synonymously. Characterization of the amylin gene and the amino acid sequence revealed close homology between amylin and calcitonin-gene related peptide (CGRP), an alternate splicing product of the calcitonin gene (Mosselman et al. 1988; Westermark et al. 1986). Amylin and CGRP form, along with adrenomedullin (AM), calcitonin (CT) and intermedin, the CT super family (Wimalawansa 1997).

After the first isolation of amylin from the pancreas, and the detection of amylin-like immunoreactivity in pancreatic islets (Johnson et al. 1988), it was later found to be colocalized with insulin in pancreatic beta-cells (Denijn et al. 1992). The observation that amylin secretion was modulated by factors also known to modulate insulin secretion, such as glucose, carbachol (Jamal et al. 1993), the amino acid arginine (Ogawa et al. 1990) or somatostatin (Mitsukawa et al. 1990) led to the assumption that amylin was co-secreted from pancreatic beta-cells with insulin. Since then, immunoreactivity has also been found in some other tissues such as the gut, especially in the pyloric antrum (Asai et al. 1990), the nervous system (Mulder et al. 1995; Skofitsch et al. 1995), osteoblasts (Gilbey et al. 1991) and in rat and human placenta (Caminos et al. 2009). However, expression levels in these tissues are much lower than in the pancreas.

The amylin receptor consists of a calcitonin receptor that is associated with one of three receptor activity modifying proteins (RAMPs). This association leads to an alteration in receptor pharmacology from CT-preferring to amylin-preferring (Muff et al. 1999; Zumpe et al. 2000).

1.2.2 Influence on nutrient fluxes

Amylin plays a very important role in the control of gastrointestinal nutrient transit and absorption. Being secreted in response to nutrient stimuli, its main action is to slow glucose

absorption and, consequently, the rise in postprandial plasma glucose (Kolterman et al. 1995). This effect is mediated by different actions of amylin, i. e. suppression of glucagon secretion (Gedulin et al. 1997) that leads to lower endogenous glucose production (Unger and Orci 1977), delayed gastric emptying (Gedulin et al. 2006; Kong et al. 1997; Young et al. 1995) and inhibition of gastric acid secretion (Guidobono et al. 1994). The effect on gastric functions is prevented by hypoglycemia (Gedulin and Young 1998), which is thought to be a "fail-safe" reflex to prevent insufficient nutrient availability during hypoglycemia (Young 1997).

There is strong evidence that central sites mediate the gastric effects of amylin, namely the area postrema (AP) in the hindbrain, which displays a very high binding density for amylin. Furthermore, lesion of the area postrema abolishes the gastric effects (Young 1997), but importantly also the anorectic effect of amylin (Lutz et al. 1998).

1.2.3 Effects on food intake

Amylin acts as a classical satiation signal, as it is released during meals and dose-dependently reduces meal size after intraperitoneal and subcutaneous injection. Hepatic portal infusion during spontaneous meals inhibited feeding within minutes and led to a reduction in meal size and duration (Lutz et al. 1995b). In addition, direct amylin infusion into the AP reduced food intake significantly in fasted rats. Further, strong evidence for a physiological relevance of the satiating effect of amylin was provided by the application of the amylin antagonist AC 187. AC 187 increased food intake, mainly by increasing meal size, after peripheral injection or after central infusion into the AP (Mollet et al. 2004; Reidelberger et al. 2004). The anorectic effect of amylin is not based on a conditioned taste aversion or unspecific effects such as a reduction in drinking; it therefore seems to be specific (Morley et al. 1997).

1.2.4 Amylin and diabetes mellitus

Type 1 diabetes mellitus is presumably caused by an autoimmune destruction of pancreatic β cells and is therefore characterized by an absolute deficiency in insulin secretion. As amylin is co-secreted with insulin, patients suffering from type 1 diabetes also show a deficiency in amylin secretion. Therefore, amylin agonists in combination with insulin are used for the treatment of type 1 diabetes, mainly due to the inhibitory effects of glucagon

secretion and gastric emptying (Edelman and Caballero 2006; Heptulla et al. 2005; Schmitz et al. 2004).

Type 2 diabetes mellitus (T2DM) is a multifactorial disease influenced by genetic, environmental and endogenous factors (Hayden and Tyagi 2001). It is characterized by insulin resistance and, in a progressive stage, β-cell failure (Ferrannini 1998). In patients with T2DM, islet amyloid is a typical finding present in the pancreatic islets of the vast majority (Oosterwijk et al. 1995), and is thought to play an important role in the pathogenesis of beta-cell failure.

1.3 Area postrema

The area postrema is located on the dorsal surface of the medulla oblongata at the caudal end of the fourth ventricle. It belongs to the sensory circumventricular organs (CVO), which are characterized by fenestrated capillaries, high permeability, extensive vascularization and their location around the third and fourth ventricle (Gross 1992; Krisch et al. 1978). Together with the organum vasculosum of the lamina terminalis (OVLT) and the subfornical organ (SFO), the AP belongs to the so-called sensory CVOs (Johnson and Gross 1993).

Other brain regions are protected from circulating molecules, such as hormones and glucose, but also toxins, and from changes in osmolarity and electrolytes by a functional blood-brain barrier (BBB), which is essential for the maintenance of neuronal signaling (Abbott 2004; Abbott et al. 2006). Due to the lack of the BBB in sensory CVOs, they are ideally situated to act as an interface between the periphery and the brain and represent target sites for circulating humoral signals. This is supported by the high density of binding sites for different peptide hormones (Barberis and Tribollet 1996; Gebke et al. 2000; Krisch 1992; Mangurian et al. 1999; Mendelsohn et al. 1987; Nakajima et al. 1986; Sexton et al. 1994; Weindl et al. 1992) in all sensory CVOs and by the ability of most of these peptides to evoke electrophysiological responses in neurons of sensory CVOs (Carpenter et al. 1983; Ferguson 1991; Gutman et al. 1988; Riediger et al. 1999; Schmid et al. 1998; Yang and Ferguson 2002). To exert their important regulatory effects on various physiological functions, CVOs are connected to other brain regions by numerous projections, mostly to essential autonomic centers in the hypothalamus and the medulla oblongata (Armstrong et al. 1996; Ferguson et al. 1984; Lind 1988; Lind et al. 1982; Miselis 1982; Miselis et al. 1979; Weiss and Hatton 1990).

The AP has major efferent projections to the nucleus of the solitary tract (NTS) (Shapiro and Miselis 1985), which receives inputs from visceral (Kalia and Sullivan 1982; Rinaman et

al. 1989) and cardiovascular (Palkovits and Zaborszky 1977; van Giersbergen et al. 1992) afferents. It also projects to the parabrachial nucleus (PBN) (Lanca and van der Kooy 1985), which receives gustatory and viscerosensory inputs (Hermann and Rogers 1985). Both the NTS and the PBN are strongly connected to other brain regions, amongst others the paraventricular nucleus of the hypothalamus (PVN) (McKellar and Loewy 1981) and other hypothalamic structures (Sakumoto et al. 1978), the bed nucleus of the stria terminalis (Sofroniew 1983) and the central nucleus of the amygdala (Ricardo and Koh 1978). Minor neuronal connections from the AP project to the nucleus ambiguus and the dorsal motor nucleus of the vagus nerve, which are both involved in the control of heart rate and cardiac function (Wang et al. 2001), and to dorsal regions of the tegmental nuclei (Shapiro and Miselis 1985).

The AP also receives afferent inputs from mostly the same regions it projects to. Major afferents originate from the NTS and PBN; other inputs come from the PVN and the vagus nerve (Papas and Ferguson 1990; Vigier and Rouviere 1979).

In summary, the AP is a highly interconnected brain area and sends and receives projections to a number of other brain regions, which are part of different autonomic circuits. It holds a key position in integrating peripheral and central signals and has been shown to be, together with the NTS, the major site of abdominal sensory inputs (Hyde and Miselis 1983)

1.3.1 Functions of the AP

The AP plays a crucial role in the control of various autonomic physiological functions, including emesis, taste sensitivity, cardiovascular control and, most important for this study, the control of eating.

Borison (Borison 1974; Borison and Wang 1953) first discovered the existence of chemoreceptors in the AP that respond to certain drugs by a stimulation of vomiting. His findings led to the conclusion that the AP is important for the detection of ingested toxins and for their elimination from the gastrointestinal tract. This was corroborated by studies using AP lesioned animals, which did not show an emetic response to a variety of drugs (Bhandari et al. 1992; Jovanovic-Micic et al. 1989; Miller and Nonaka 1992).

Berger et al. (Berger et al. 1973) studied the formation of conditioned taste aversions (CTA), which are learned responses leading to the avoidance of food that had previously been associated with toxic effects; they showed that the AP plays a critical role in the formation of CTA by scopolamine methyl nitrate. Later studies supported this, showing the same effects

for lithium chloride (Kosten and Contreras 1989; Ritter et al. 1980) and amphetamine (Rabin and Hunt 1989).

The existence of arginine vasopressin (AVP) (Barberis and Tribollet 1996) and angiotensin II (ANGII) (Mendelsohn et al. 1987) receptors suggested a role of the AP in cardiovascular control. AVP and ANGII effects on blood pressure and heart rate were abolished in AP lesioned rats (Bishop et al. 1987; Fink et al. 1987; Undesser et al. 1985); studies on brainstem slices confirmed a role of the AP in mediating ANGII and AVP effects, as both ANGII and AVP had inhibitory and excitatory effects on AP neurons (Cai and Bishop 1995; Lowes et al. 1995).

The AP expresses a high density of binding sites for different hormones and neuropeptides involved in the control of eating, such as amylin (Sexton et al. 1994), peptide YY (Trinh et al. 1996), CCK (Carlberg et al. 1992; Hyde and Peroutka 1989), glucagon-like peptide-1 (Goke et al. 1995) and others. As indicated earlier, most of the effects of amylin on nutrient fluxes and food intake seem to be mediated by the AP (see chapters 1.2.2 and 1.2.3). In addition to the abolition of gastric and anorectic effects in AP lesioned rats (Lutz et al. 2001; Young 1997) and the direct effects of the amylin antagonist AC 187 when infused into the AP (Mollet et al. 2004), electrophysiological studies revealed an excitatory effect of amylin on AP neurons, which could also be blocked by AC 187 (Riediger et al. 2001).

Another method used for the detection of neuronal stimulation in vivo is the immunohistochemical detection of the immediate early gene product c-Fos. c-Fos is a transcription factor, which exerts either stimulatory or inhibitory effects on gene transcription. Under baseline conditions, c-Fos expression is very low in most neurons, whereas after depolarizing stimuli gene expression is rapidly induced, peaking between 60 and 90 minutes and persisting for 2 to 5 hours (Hoffman et al. 1993; Sharp et al. 1991). C-Fos is therefore a widely accepted experimental marker for neuronal activation.

In line with its excitatory effects on AP neurons, amylin also induces a strong c-Fos expression in the AP after peripheral amylin injection (Riediger et al. 2001; Riediger et al. 2004; Rowland et al. 1997). In addition to the AP, amylin also elicits a c-Fos response in the NTS-LPBN-CeA axis which transmits the excitatory amylin signal to rostral brain areas (Rowland et al. 1997). In AP lesioned rats, c-Fos expression in these areas was attenuated after amylin injection (Riediger et al. 2004), which provides further evidence for a role of the AP as a primary target site for peripheral amylin.

Together, all these studies point to a decisive role of the AP in amylin action.

1.4 The arcuate nucleus of the hypothalamus

The hypothalamus plays a key role in the control of physiological functions and behavioral patterns that ensure survival, such as the control of eating, drinking, defense and reproduction (Luiten et al. 1987). Regarding the control of eating, the hypothalamus serves as the major central site for the integration of peripheral satiation signals and adiposity signals reflecting energy stores (Elmquist et al. 2005; Minor et al. 2009). The arcuate nucleus of the hypothalamus (ARH), together with the paraventricular nucleus of the hypothalamus, is particularly important for the control of food intake and energy balance because it functions as a receptive site for these signals.

The ARH is located at the base of the third ventricle and is interconnected with the brainstem (Abbott et al. 2005; Ter Horst et al. 1989) and other hypothalamic nuclei, including the dorsomedial nucleus (DMH), the lateral hypothalamic area (LHA) and the paraventricular nucleus (PVH) (Kalra et al. 1999).

The two main populations of neurons involved in the control of feeding and energy balance have briefly been described before (see chapter 1.1.2). Activation of POMC neurons results in the secretion of αMSH, which acts on melanocortin receptors of secondary neuron populations in the PVH and other hypothalamic nuclei (Belgardt et al. 2009; Wikberg et al. 2003). The stimulation of secondary neurons leads to an increase in energy expenditure and a decrease in food intake; the exact mechanisms though, especially how this information is translated into specific motor patterns of eating, are not completely understood yet. Activation of AgRP/NPY neurons on the other hand leads to an increase in food intake by two different mechanisms. AgRP directly inhibits the activation of secondary neurons by αMSH, whereas NPY has stimulatory effects on hunger, fat storage and weight gain (Beck et al. 1992; Stanley et al. 1986; Zarjevski et al. 1993) while decreasing body temperature and energy expenditure (Billington et al. 1991; Hwa et al. 1999). POMC knockout mice, as well as POMC-deficient humans, overeat and develop extreme obesity (Yaswen et al. 1999), while acute ablation of AgRP/NPY neurons led to a decrease in food intake and body weight (Gropp et al. 2005; Luquet et al. 2005).

Both populations of neurons express receptors for leptin and insulin that seem to be directly targeted by leptin and insulin (Baskin et al. 1988; Mercer et al. 1996). Both hormones stimulate POMC neurons and inhibit AgRP/NPY neurons (Pinto et al. 2004; Ziotopoulou et al. 2000).

1.5 Amylin knockout mice

To investigate the physiological functions of endogenous amylin, *Gebre-Medhin et al.* created mice lacking amylin by a targeted deletion of the IAPP gene (Gebre-Medhin et al. 1998a). IAPP-deficient mice (*IAPP*$^{-/-}$) were born from heterozygous (IAPP$^{+/-}$) parents in Mendelian frequencies and appeared healthy; the typical distribution of insulin-immunoreactivity was indicative of normal morphology of the islet of Langerhans in adult IAPP$^{-/-}$ mice. Screening of IAPP$^{-/-}$ mice and wildtype (IAPP$^{+/+}$) controls from the age of 6 – 42 weeks showed no difference in basal glucose levels. From 30 weeks of age, IAPP$^{-/-}$ animals showed a tendency towards lower insulin levels, but the difference was not significant (Gebre-Medhin et al. 1998a). Male IAPP$^{-/-}$ mice showed an increased plasma insulin response in intravenous and oral glucose tolerance tests (IVGTT; OGTT), a faster decline in plasma glucose concentrations in IVGTT and a lower plasma glucose peak in OGTT.

In a subsequent study, the role of amylin in nociception and inflammatory response was tested in IAPP$^{-/-}$ mice. Nociceptive behavior was significantly reduced compared to controls, but this effect was not due to altered inflammatory response (Gebre-Medhin et al. 1998b). The reduced response to noxious stimuli in IAPP$^{-/-}$ mice implied a pro-nociceptive action of amylin in sensory neurons, as the inflammatory response seemed to be unaltered. Alternatively, amylin may exert trophic effects on nerve fibers involved in nociceptive transmission, which is interesting in context with the present study.

A further effect seen in amylin deficient mice was a reduction in bone mass. IAPP$^{-/-}$ males and females showed a 50 % decrease in bone mass due to a decrease in cortical and trabecular thickness and in connectivity between trabeculae, which is typical of osteoporosis. All hormonal and metabolic parameters measured were normal; therefore bone effects were not secondary to metabolic changes but probably specific to the deficit in endogenous amylin (Dacquin et al. 2004).

While food consumption did not differ significantly between groups, male IAPP$^{-/-}$ mice showed a significant increase in body mass between the age of 18 weeks (Gebre-Medhin et al. 1998a) and about 4 months compared to wildtypes, but not in mice older than 4 months (Lutz 2006).

Recent studies from our group showed a significant reduction in food intake shortly after amylin injection in adult IAPP$^{+/+}$ and in IAPP$^{-/-}$ mice. IAPP$^{-/-}$ mice therefore seem to be similarly sensitive to exogenously administered amylin and its inhibitory effects on eating as control mice, which is in principle consistent with the findings of *Gebre-Medhin* and colleagues about basal food intake (unpublished data).

1.6 Leptin-deficient ob/ob mice

In 1949, *Ingalls et al.* discovered some young mice in a breeding stock that showed a very plump phenotype. With the occurrence in more litters, it became clear that a hereditary mutation was the most likely cause of this phenotype. Affected mice gained weight more rapidly than their littermates and became massively obese, which is why the mutation was called obese and designated by the symbol *ob* (Ingalls et al. 1950). In 1994, *Zhang et al*. cloned and sequenced the mouse *ob* gene and the human homologue; they were also able to identify its product, the Ob protein, which today is better known as leptin (Zhang et al. 1994). Daily intraperitoneal injections of recombinant leptin led to a reduction in body weight, food intake and body fat mass in *ob/ob* mice (Halaas et al. 1995; Pelleymounter et al. 1995).

Mice carrying another gene mutation, diabetes (*db*), which leads to a nearly identical phenotype as the *ob* mutation (Hummel et al. 1966), showed massively elevated circulating leptin levels (Halaas et al. 1995). As they did not show a reduction in body weight or food intake after leptin administration (Halaas et al. 1995), it was assumed that they might be resistant to leptin; this was confirmed by the finding that the *db* gene encodes for the leptin receptor (Chen et al. 1996; Chua et al. 1996).

1.6.1 Neurotrophic effects of leptin

Ahima and colleagues reported about the existence of a postnatal leptin surge in mouse pups during their first week of life (Ahima et al. 1998). This was an unexpected finding because the elevated leptin levels were not associated with a reduction in food intake. This was interpreted as an insensitivity of the neonatal brain to leptin (Mistry et al. 1999). As circulating hormones, such as thyroid hormone (Bernal, 2002; Oppenheimer et al., 1987) and sex hormones (Madeira and Lieberman, 1995; McEwen et al., 1986; Simerly, 2002), have been known to strongly influence brain development perinatally, especially in the limbic system and the hypothalamus (Bernal 2002; Madeira and Lieberman 1995; McEwen et al. 1986; Oppenheimer et al. 1987; Simerly 2002), it was speculated that leptin might also function as an early postnatal developmental signal in neonates (Ahima et al. 1999; Ahima and Hileman 2000; Steppan and Swick 1999). This view was supported by the finding that brains of *ob/ob* mice were smaller and weighed less than brains of normal mice. Daily leptin administration for two weeks increased brain weight and cell number, indicating a possible defect in brain development in *ob/ob* mice (Steppan and Swick 1999).

Bouret et al. used the lipophilic fluorescent tracer DiI (1,1'-dioctadecyl-3,3,3',3'-tetramethylindocarbocyanine perchlorate) which labels axonal projections (Honig and Hume 1989), to investigate the developmental role of leptin in projections from the ARH to other hypothalamic nuclei. They showed that projections to the PVH, the DMH and the LHA developed from postnatal day 5 (P5) to P16. Most interestingly, this coincided with the time of the postnatal leptin surge (Bouret et al. 2004a; b).

Projections in *ob/ob* mouse pups of different ages were profoundly underdeveloped compared to their wild-type littermates. This disruption seemed to be permanent as a difference could still be seen in adult mice. Daily leptin treatment from of neonatal *ob/ob* mouse pups P4 to P12 led to a reversal of the effect, i.e. the density of ARH to PVH was similar to wildtype control mice. Further, incubation of brain slices containing the ARH with leptin induced the growth of neurites from the ARH, suggesting a direct action of leptin on arcuate neurons to stimulate axon growth. However, leptin treatment of adult mice was unable to reconstitute a normal neurocircuitry (Bouret et al. 2004b). These findings clearly demonstrate that leptin plays an important role in the development and programming of neural feeding circuits in the hypothalamus of neonatal mouse pups, and that the time window for leptin to exert this effect is limited to the early postnatal phase.

1.7 Aim of the study

In addition to its effects of ingestive behavior and gastric function, amylin exerts trophic effects on the fetal and postnatal kidneys, where it stimulates proliferation of proximal tubule cells that are mainly responsible for sodium and water reabsorption (Harris et al. 1997; Wookey et al. 1998). It furthermore has effects on bone formation and mineralization by stimulating the proliferation of osteoblasts and inhibiting osteoclast activity (Cornish et al. 1995). Amylin expression is already present in the fetal pancreas (Mulder et al. 1997), which suggests a potential developmental role of amylin during ontogeny.

Based on the findings that leptin exerts trophic effects on the formation of projections from the ARH to other hypothalamic nuclei (Bouret et al. 2004b), our group recently investigated whether amylin, similar to leptin, has neurotrophic effects on neuronal projections in the CNS. As the AP has been identified as amylin's central site of action (see chapter 1.3.1), projections from the AP to the NTS were analyzed first, using and adapting the DiI axonal labeling technique described by *Bouret et al*. (2004a,b) We showed a significant reduction of fiber projections from the AP to the NTS in $IAPP^{-/-}$ mice on postnatal day 10

(P10) and a tendency towards lower fiber density on P14. We also found a reduced fiber density in P14 $IAPP^{+/+}$ mice compared to P10 $IAPP^{+/+}$, indicative of neural remodeling processes (unpublished data).

The first aim of the current study was to analyze additional data of male P14 mice, which allowed us gender-specific evaluation. Further, we wanted to determine the consequences of amylin deficiency on neural circuits from the AP to the NTS in adult mice. Because receptor upregulation compensatory to hormone deficiency has been described for different hormones including leptin (Huang et al. 1997), we also analyzed the density of calcitonin receptors in the AP of adult mice. With the objective of investigating amylin's effect on ARH-PVH projection development in a future study, our second aim was the establishment of DiI implantation into the ARH as described by *Bouret et al.* (2004a,b).

Furthermore, we hypothesized that leptin may also influence the development of AP projections in the hindbrain; for this reason we investigated AP-NTS projections in P14 *ob/ob* mice.

We wanted to answer the following questions:

- Does the neurotrophic function of amylin observed in early postnatal mice have an impact on the neuroanatomy of adult $IAPP^{-/-}$ mice? Are there functional consequences in signal transduction in the AP/NTS region?

- Does amylin have an influence on calcitonin receptor density in the AP of adult mice?

- Does leptin also have neurotrophic effects on the development of projections from the AP to the NTS?

2 Materials and methods

2.1 Animals

2.1.1 Generation of amylin knockout mice

The generation of amylin *ko* mice was first described by Gebre-Medhin et al. (Gebre-Medhin et al. 1998a). To create amylin deficient mice, a 10.5 kbp fragment containing the murine IAPP gene was cloned from a genomic mouse Balb/c library (Stratagene) by plaque hybridization to the human IAPP cDNA. The replacement of an 890 bp SphI/BamHI fragment containing part of exon 3, and internal to a 3.46 kbp HindIII/XbaI fragment, by a phosphoglycerate kinase promoter-driven neomycin resistance gene (neo)-selection cassette resulted in the deletion of all sequence encoding the 37-amino-acid IAPP peptide. The resulting DNA construct was fused with a 5.1 kbp XbaI/SalI fragment and cultured mouse 129Ola/sv embryonic stem (ES) cells were transfected with the product. ES cells were screened for recombinant clones and chimeric mice were generated.

The screening probe was a 1.5 kbp EcoRI-HindIII genomic DNA fragment containing the second exon of the IAPP gene. The deletion of the sequence coding for IAPP in the targeted IAPP allele was confirmed using exon 3-specific oligonucleotide probes bp 89-179 and bp 170-253 of the published mouse IAPP sequence. These probes were radio labeled using 5'GTTGCTGGAA3' and 5'CCTAGGGGAC3', respectively, as primers in the presence of [^{32}P]dCTP, unlabelled dATP, dTTP, and dGTP and the Klenow fragment of DNA polymerase I. Hybridizations were carried out at high stringency.

We did not generate the amylin knockout mice ourselves for our studies, but our breeders were supplied by *Amylin Pharmaceuticals, Inc.,* USA. The breeder mice were derived from frozen embryos of amylin knockout mice of the original mouse strain developed by Gebre-Medhin.

2.1.2 Animal breeding and housing

In order to minimize any prenatal and postnatal environmental influences on projection development, it was of great importance for the present study to use IAPP$^{+/+}$ and IAPP$^{-/-}$ littermates. For this reason, homozygous amylin knockout mice (provided by Amylin Pharmaceuticals, Inc., USA) were crossbred with C57BL/6 wildtype mice (Jackson Laboratories, Maine, USA), thus establishing a heterozygous (IAPP$^{+/-}$) F1 generation.

Heterozygous breeding pairs were used to create an F2 generation, which was, according to the Mendelian inheritance, expected to comprise 25% IAPP$^{+/+}$ *wildtype (wt)*, 50% IAPP$^{+/-}$ *heterozygous (het)* and 25% IAPP$^{-/-}$ *knockout (ko)* mice **(Fig.1)**.

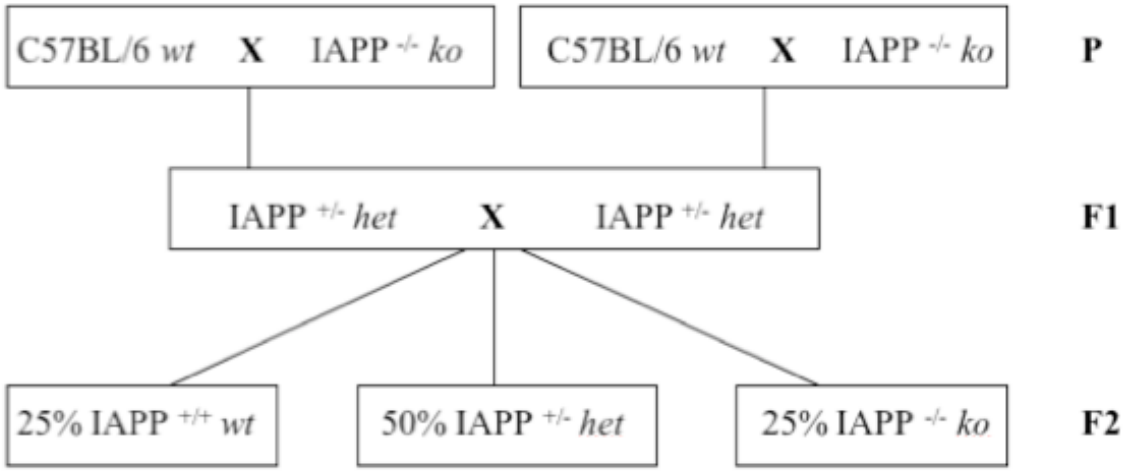

Figure 1 Breeding of transgenic mice and expected distribution of genotypes in the F2 generation.

C57BL/6 mice were obtained from *Jackson Laboratories*, USA; IAPP$^{-/-}$ mice from *Amylin Pharmaceuticals, Inc.,* USA.

For DiI tracing studies, male *ko* and *wt* littermates were used on postnatal day 14 (P14) and around postnatal day 60 (±2 days; P60) to investigate the development of projections from the AP to the NTS and from the ARH to the PVH, respectively. Male and female littermates were used on P60 for immunohistochemistry for the detection of amylin-induced c-Fos expression. Animals from litters smaller than five or larger than ten pups were excluded from the study in order to minimize the likelihood that differences in individual development due to litter size account for the effects characterized in the current study. Experiments were in accordance with the guidelines of and approved by the Veterinary Office of the Canton Zurich, Switzerland.

All animals were kept in standard macrolon cages; litters were housed in the same cage with their parents until they were used for the experiments or until weaning on P21. The breeding pairs and weaned mice had *ad libitum* access to food (standard pellet chow, #3430, Kliba Nafag AG, Gossau, Switzerland) and water. Animals were kept under an artificial 12:12 h light / dark cycle with lights off at 6 pm.

2.2 Dil fiber labeling

2.2.1 Perfusion and tissue fixation

2.2.1.1 Material

- Micro eye scissor (85mm, 3 3/8", B. Braun medical AG, Tuttlingen, Germany)
- Micro forceps (Jeweler Type, 0.3mm, angled, 110mm, 4 3/8", B. Braun Medical AG)
- Canulae (Terumo, 26G x ½", Leuven, Belgium)
- Three-way stopcock (B. Braun Medical AG) with flexible infusion tubes
- Mini-clamp to fix perfusion canula
- Syringes (Omnifix 1ml, 20ml, Braun Melsungen AG, Melsungen, Germany)
- 4% paraformaldehyde in sodium phosphate buffer **(Tab. 1)**
  - Paraformaldehyde purum ≥95.0% (Sigma-Aldrich, Saint Louis MO, USA)
  - Sodium dihydrogen phosphate monohydrate (Sigma-Aldrich)
  - Sodium phosphate dibasic dihydrate (Sigma-Aldrich)
- 0.9% NaCl
- Pentobarbital sodium (50mg/ml, Kantonsapotheke Zürich KAZ, Switzerland)
- Tribromoethanol **(Tab. 2)**
  - 2,2,2-Tribromoethanol (Sigma-Aldrich)
  - Ter-amyl alcohol-gold label reagent (Sigma-Aldrich)
  - Ethanol 100%
  - 0.7% Saline

Table 1 4% Paraformaldehyde in sodium phosphate buffer

Stock solution	Substance	Concentration [g/l]	End concentration [M]
I	$NaH_2PO_4 \cdot H_2O$	27.6	0.2
II	$Na_2HPO_4 \cdot 2H_2O$	35.85	0.2
Working Solution: 500ml ddH_2O + 40g Paraformaldehyde + 2 pellets of NaOH were stirred and heated until complete dissolving, then filtered into 115ml of stock I and 385ml of stock II. The pH was adjusted to 7.4 using HCl.			

Table 2 Tribromoethanol

	Preparation
Stock solution	100g 2,2,2-Tribromoethanol dissolved in 62.5ml of ter-amyl alcohol-gold label reagent (Kantonsapotheke Zürich KAZ)
Working solution	2ml TBEtOH + 8ml EtOH 100% + 90ml NaCl 0.7%

2.2.1.2 Anesthesia and transcardial perfusion

Adult mice were deeply anesthetized intraperitoneally with pentobarbital sodium (200mg/kg). For mouse pups, tribromoethanol (0.15-0.2ml/pup) was used because they are extremely sensitive to pentobarbital and the risk of respiratory arrest is much higher in mouse pups than in adults. Tribromoethanol provides surgical tolerance within five minutes, good analgesia and deep anesthesia for approximately one hour. In addition, respiratory depression is lower with tribromoethanol than with pentobarbital, which is crucial for the anesthesia of neonatal pups.

The injection site was paramedian between teats and knee flexure with the needle pointing at the contralateral elbow. Loss of the flexor reflex of the hind leg was tested with a forceps to confirm anesthetic depth.

After confirming a deep level of anesthesia, mice were fixed in a dorsal position. The skin of the thorax and the abdomen was dissected and an incision was made at the xiphoid process. The abdominal wall was cut along the costal arcs without injuring the liver to clearly visualize the diaphragm. After removing the diaphragm, the thoracic cavity was opened by cutting the ribs and the heart was exposed. A small incision with a micro eye scissor was made into the left ventricle to facilitate the insertion of a blunt 26 G canula; after fixing the canula with a mini-clamp the right atrium was cut. Exsanguination was then performed by infusing a 0.9% NaCl solution into the left ventricle with a hydrostatic pressure of 150cm for 2 minutes, followed by the perfusion with ice-cold paraformaldehyde solution (PFA) for 6 minutes. After fixation, the mice were decapitated and the skullcap was quickly removed. Brains were immediately transferred into cold PFA and kept for 10 days at 4°C for postfixation.

2.2.2 DiI Implantation

2.2.2.1 Material

- DiI C_{18} (1,1'-dioctadecyl-3,3,3',3'-tetramethylindocarbocyanine perchlorate, Molecular Probes, Eugene, OR)
- Micrometer benchmark (100 x 0.01mm, Pyser-SGI Limited, Kent, UK)
- Insect pin (Minutien, 0.1mm, Bauer Handels GmbH, Adetswil, Switzerland)
- Zoom stereomicroscope (Wild M8, Leica Microsystems, Nussloch, Germany)
- Methylene blue
- 3 way micromanipulator (SD Instruments, Grants Pass, OR, USA)
- Dual arm fiber optic illuminator (Intralux® 4000, Volpi AG, Schlieren, Switzerland)
- Micro forceps (Jeweler Type, 0.3mm, angled, 110mm, 4 3/8", B. Braun Medical AG)

2.2.2.2 Implantation into the AP

After the brains had been postfixed for 10 days, they were transected at the mid rostrocaudal level. The hindbrains were processed directly, while the forebrains were embedded in agarose before they were trimmed to expose the implantation site (see below). Methylene blue was used to stain and identify morphological structures of the hindbrain. The cerebellum was carefully dissected with two micro forceps under a stereomicroscope until the area postrema (AP) could be identified. A DiI crystal, which had been selected before and checked for size and shape, was then implanted into the AP. Selected crystals had a round, symmetric shape and were about 10 and 15 µm in diameter for P14 and P60 mice, respectively.

The crystal was first placed at the intended implantation site on the surface of the AP, using a micromanipulator. It was then carefully pushed into the tissue with an insect pin. The implantation site was in the center of the dorsal AP surface and the crystal was placed about 50µm under the surface **(Fig. 2 + 3)**. After implantation, brains were stored in 4% PFA at 37°C and the tracer was allowed to migrate for 10 days in the dark.

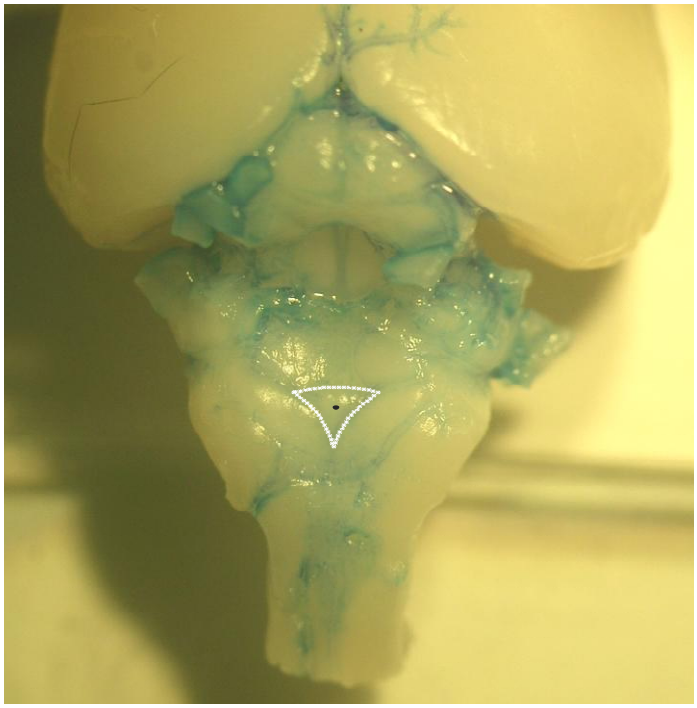

Figure 2 Implantation site of DiI crystals

Brainstem after the removal of the cerebellum and stained with methylene blue.
Dotted line = AP surface, black dot = implantation site

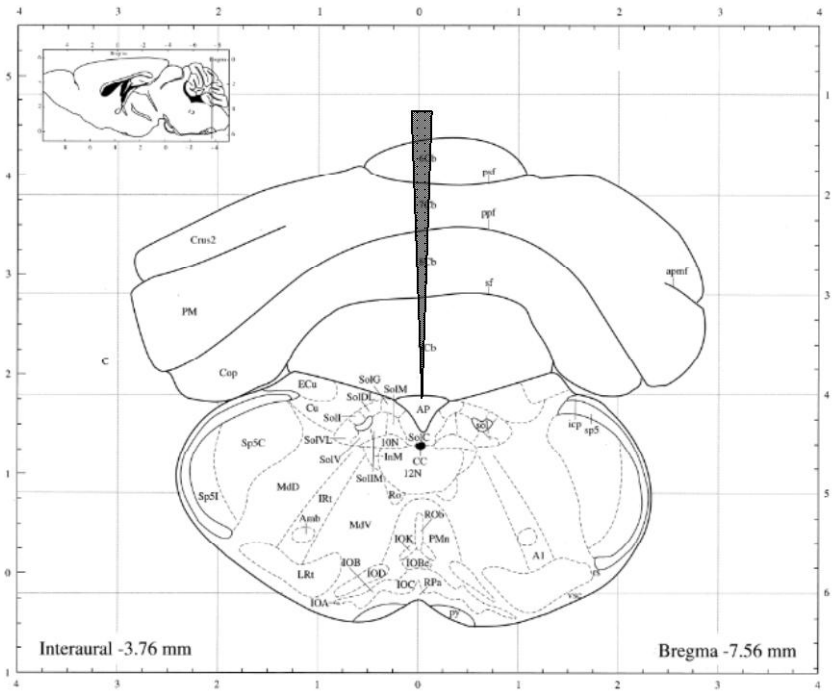

Figure 3 Implantation site of DiI crystals in the AP illustrated in a coronal diagram of the brainstem (adapted from Paxinos and Franklin, 2004)

2.2.2.3 Implantation into the ARH

Forebrains had to be embedded in 3% agarose and sliced from caudal to rostral with a vibratome (see chapter 2.2.3) until the arcuate nucleus was accessible for implantation. During slicing, single sections were collected and evaluated under the stereomicroscope after methylene blue treatment to determine bregma positions. Crystals (diameter about 25 µm) were then implanted unilaterally in the center of the ARH **(Fig. 4)**, using the same technique as in the AP. The tracer was allowed to diffuse for six weeks in the dark at 37°C.

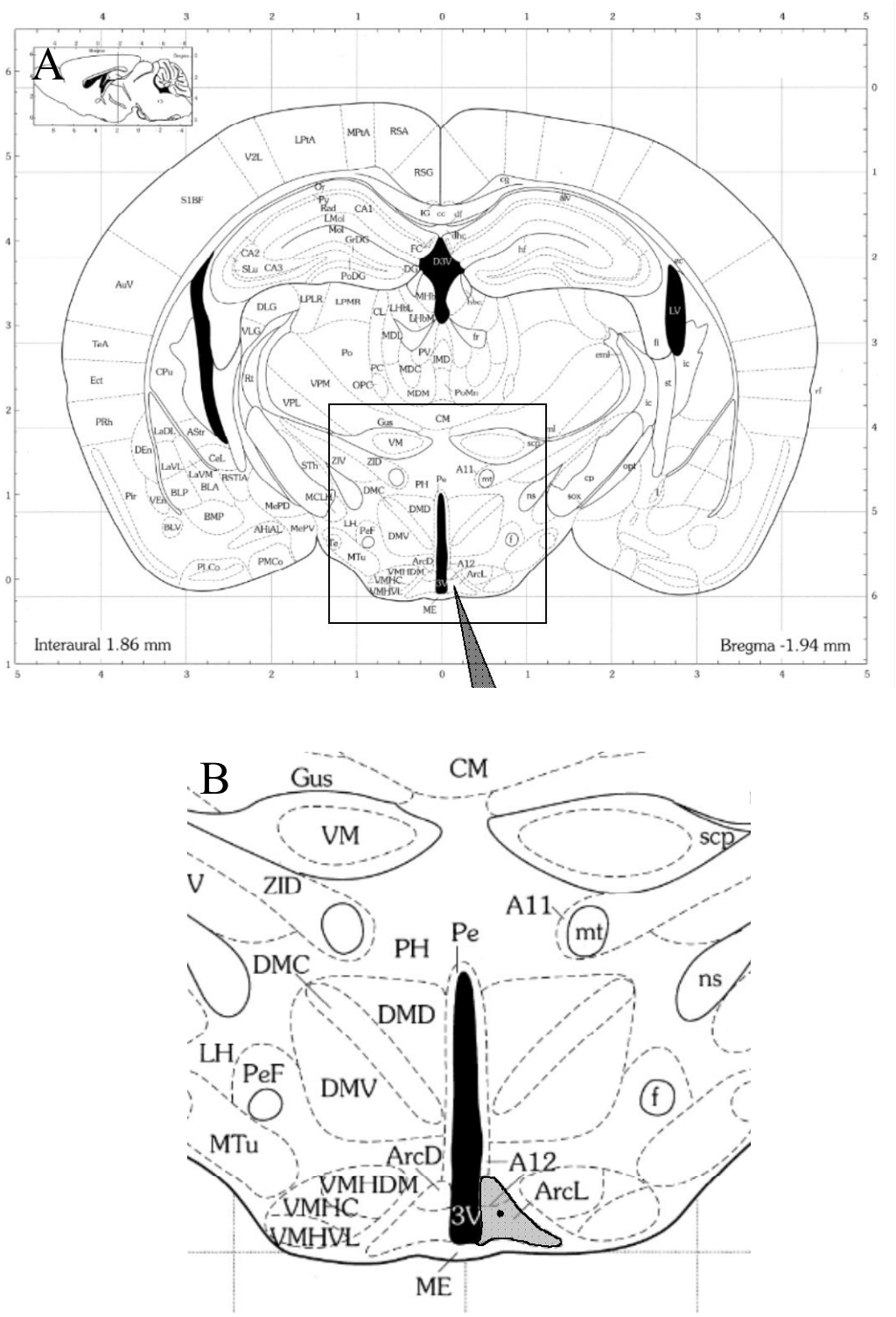

Figure 4 Implantation site of DiI crystals in the ARH illustrated in a coronal diagram of the forebrain (adapted from Paxinos and Franklin, 2004; image specifications corresponding to adult mice)

A The crystal was implanted along the rostrocaudal axis into the center of the ARH

B Detail magnification of A (black box); *shaded field =ARH, black dot = implantation site*

2.2.3 Brain slicing

2.2.3.1 Material

- Vibratome (Leica VT 1000s, Leica Microsystems)
- Agarose (#820723, MP Biomedicals, Inc., Solon, Ohio, USA)
- KPBS buffer **(Tab. 3)**
- Multi-well plate
- Soft paint brush
- Poly-L-lysine-coated (sigma-Aldrich, Inc.) glass slides (Thermo Scientific, microscope slides 76 x 26mm, Menzel GmbH & Co. KG, Braunschweig, Germany)
- 65% KPBS buffered glycerol
- Microscopic cover slips (24 x 50mm, Menzel GmbH & Co. KG)
- Rapid mounting medium (Entellan®, Merck, Darmstadt, Germany)

Table 3 KPBS buffer (0.02M)

Substance	Weight [g]	
KH_2PO_4	9.7	Dissolved in 20.58l ddH_2O to final concentration of 0.02M
K_2HPO_4	56.6	
NaCl	178.2	

2.2.3.2 Vibratome slicing

10 days after DiI implantation, hindbrains were embedded in 3% agarose, assuring an upright and symmetric position. Forebrains were sectioned after an incubation time of six weeks after implantation. After trimming and fixing the agarose blocks with superglue, a vibratome was used to cut 80 µm thick coronal sections through the brainstem and the hypothalamus. Hindbrains were sliced approximately between *bregma* -7.08mm and -8.24mm and forebrains between *bregma* -0.46mm and -1.70mm (*bregma* levels corresponding to adult mice, see Fig. 3. + 4.).

A soft paint brush was used to collect the brain slices, which were kept in KPBS until mounting onto poly-L-lysine-coated glass slides. The slices were covered with 65% KPBS buffered glycerol before the coverslips were put on the glass slides and fixed with Entellan®. Slides were stored at 4°C in the dark to reduce tracer fading.

2.2.4 Fluorescence microscopy

2.2.4.1 Material

- Fluorescence microscope (Zeiss Axioskop 2, upright epifluorescence microscope, Zeiss Co., Oberkochen, Germany)
- Fluorescence filter set 43 (Zeiss Co., excitation BP 545/25nm, emission BP 605/70nm)
- Microscopy digital camera (Axiocam HS, Zeiss Co.)

2.2.4.2 Microscopy

Fluorescence microscopy was used to assess successful crystal implantations and symmetric diffusion of the tracer. This was important to eliminate variation in fiber density due to abnormal diffusion or a loss of the crystal during the incubation period. Any slides that did not meet the following criteria were excluded from further analysis.

- Successful crystal implantation: Some crystals got lost during the incubation time or were implanted too superficially. For this reason, it was first checked whether the crystal was implanted deeply enough into the tissue (see **Fig. 3 + 4**).

- Symmetric crystal implantation: The symmetry of implantations was only checked in the AP, where the crystal had to be implanted exactly in the midline in order to diffuse symmetrically. As the implantation in the ARH was unilateral, it was not necessary to confirm symmetry for the entire ARH.

- Restricted tracer diffusion area: In addition to migrating along fibers, the tracer also diffused unspecifically into the surrounding tissue. This unspecific signal had to be restricted to the AP and the ARH, respectively.

- Intact tissue: Slices with damaged tissue in the AP/NTS or ARH/PVH were excluded from further analysis.

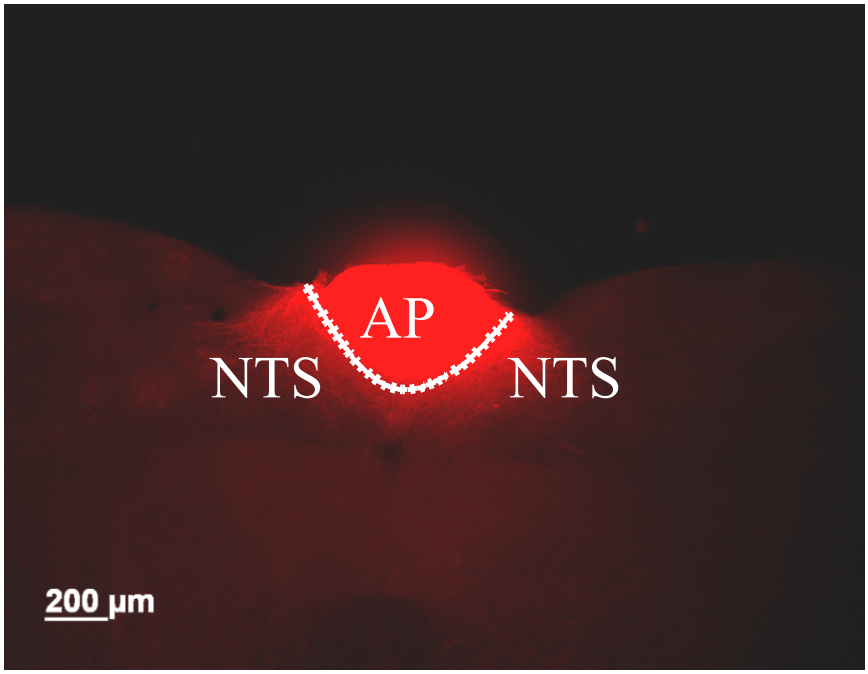

Figure 5 Fluorescence microscopic image showing an example of a successful implantation with symmetric and restricted tracer diffusion area

AP = Area postrema, NTS = Nucleus of the solitary tract, dotted line = boundary of the AP

The fluorescence microscope was equipped with an adequate filter set (fluorescence filter set 43, Zeiss Co.) for the visualization of DiI fluorescence. Excitation and emission spectra of DiI and the filter set are shown in **Fig. 6**. A digital camera was used to take pictures in different magnifications.

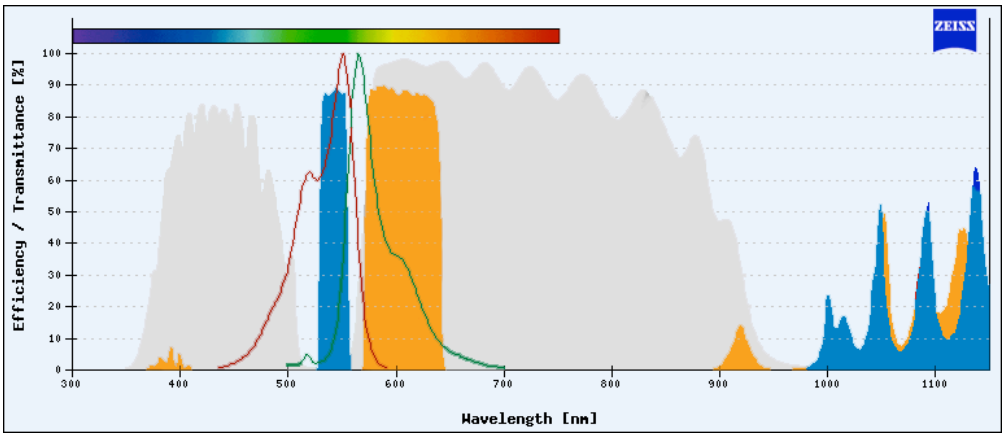

Figure 6 Spectral range of DiI tracer and filter set 43 (adapted from Zeiss Co.)

Red curve = excitation (551nm); green curve = emission (565nm) of DiI tracer
Blue area = excitation (BP 545/25nm); orange area = emission (BP 605/70); grey area = beamsplitter (FT 570nm) of filter set 43

2.2.5 Confocal laser microscopy

2.2.5.1 Material

- Confocal laser microscope (Leica SP2 AOBS, Leica Microsystems, Wetzlar, Germany)
- 63x glycerol objective (Leica, HCX PL APO lbd. BL 63x 1.3 CORR)
- 20x multi objective (Leica, HC PL APO lbd. BL 20x 0.7 IMM/CORR)

2.2.5.2 Scanning

DiI-labeled fibers of one section per brain were scanned with a confocal laser microscope. Images of the NTS region **(Fig. 7)** and the PVH were collected approximately at *bregma* -7.8 and *bregma* -0.98 (corresponding to adult mice), respectively, to analyze projections from the AP to the NTS or from the ARH to the PVH. Image stacks consisted of 75 single images with a thickness of 0.8 µm each.

For excitation, a Helium-Neon laser with a wavelength of 543nm was used; emission was detected by PMT2 between 570 and 620nm. Further settings were adjusted as follows:

- Laser HeNe 543nm; 83%
- Airy 1 pinhole 232.43µm
- Scan averaging 6
- Series a 60µm thick block was scanned with a 0.8µm step length
- Gain adjusted manually, approximately 600
- Offset adjusted manually, approximately -10

Gain and offset were adjusted manually depending on the individual signal intensity to optimize the signal:noise ratio.

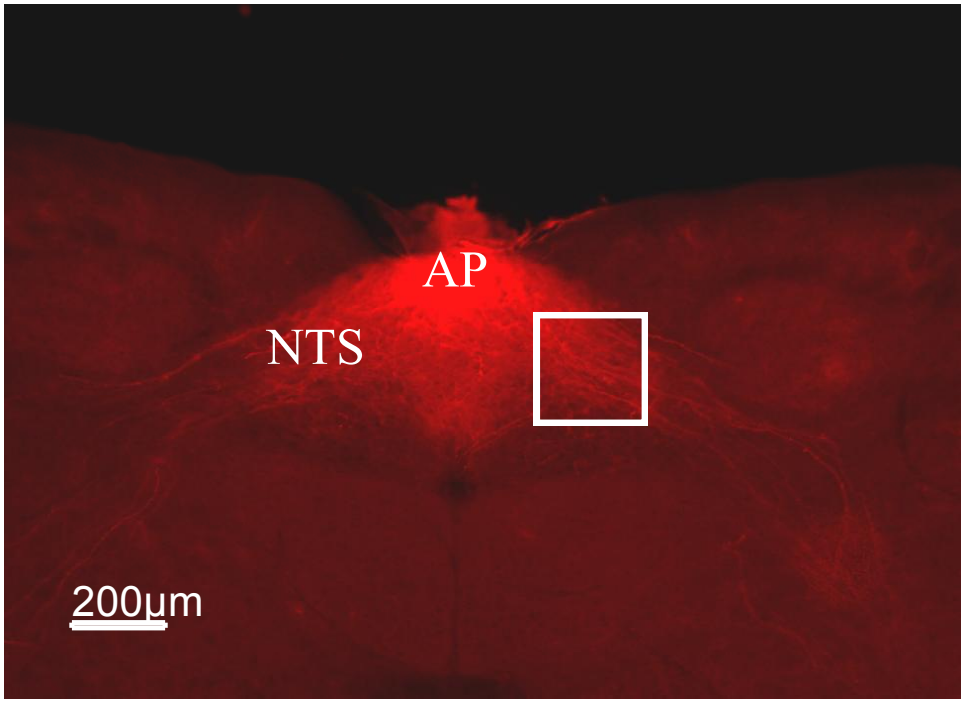

Figure 7 Fluorescence microscopic image illustrating the confocal scanning area in the NTS

AP = Area postrema; NTS = Nucleus of the solitary tract; white box = scanning area

2.2.6 Quantitative analysis

Image stacks were imported into the analysis application of the image analysis software (Imaris Version 6.4.0, Bitplane, Zurich, Switzerland). After three-dimensional reconstruction and volume rendering, the filament tracer application was used to analyze fiber density. Briefly, an autopath algorithm was used to generate filaments by connecting starting and seed points based on local intensity contrast. The largest diameter of starting points was set to 8µm, the thinnest of seed points to 0.931µm, spine detection was disabled and the signal range was adjusted manually by thresholding. Fibers were then skeletonized to a diameter of one pixel to allow the software to calculate different parameters, among them the total fiber length in the entire volume of the image stack ($3.4x10^{-3}mm^3$).

2.3 Immunohistochemistry

Immunohistochemical studies for c-Fos and calcitonin receptors were conducted in $IAPP^{-/-}$ and $IAPP^{+/+}$ animals around postnatal day 60. For the c-Fos study, adult male mice were fasted for twelve hours before receiving a subcutaneous injection of 50µg/kg amylin

(Bachem, Bubendorf, Switzerland). The animals were perfused two hours after the injection. Due to a lack of male IAPP$^{-/-}$ mice, untreated adult female mice were used for the CTR studies. They were neither fasted nor pretreated in any way.

2.3.1 Perfusion and tissue fixation

Perfusion for immunohistochemistry was conducted as described in chapter 2.2.1, with a few adaptations made in the protocol. Exsanguination was performed using 0.1M phosphate buffer (PB; **Tab. 4**), and the pH level of PB and PFA was set to 7.2 instead of 7.4. After postfixation in PFA for two hours at 4°C, brains were left for two days in 20% sucrose, dissolved in 0.1M PB, for cryoprotection.

Table 4 0.1M phosphate buffer

Stock solution	Substance	Concentration [g/l]	End concentration [M]
I	$NaH_2PO_4 \cdot H_2O$	27.8	0.2
II	$Na_2HPO_4 \cdot 2H_2O$	35.6	0.2
95ml of stock I and 405ml of stock II were stirred and diluted with 500ml ddH_2O to get 1l of 0.1M PB. After cooling the solution to 4°C, pH level was set to 7.2 using HCl. 20ml of 0.1M PB and 4g of sucrose per brain were used for the 20% sucrose solution.			

2.3.2 Brain slicing

2.3.2.1 Materials

- Cryostat (Leica CM 3050 S, Leica Microsystems)
- Forceps (B. Braun Medical AG)
- Freezing medium (Tissue Freezing Medium®, Leica Microsystems)
- Adhesive glass slides (Superfrost® Plus, Menzel GmbH & Co. KG)
- Dry ice
- Hexane

2.3.2.2 Slicing

After cryoprotection in sucrose solution the brains were rinsed with buffer solution to wash off the sucrose. They were transected at the mid rostrocaudal level before putting them into hexane on dry ice for three minutes. Using a cryomicrotome, the AP/NTS region of frozen brains was sliced into two series of 20µm sections, using adhesive glass slides to collect them. The slides were stored at -20°C until further processing.

2.3.3 Immunohistochemistry for c-Fos

2.3.3.1 Materials

- Phosphate buffered saline **(Tab. 5)**
- Triton® X-100 (Sigma-Aldrich)
- Normal goat serum (Jackson Laboratories)
- Avidin/Biotin blocking kit (Vector Laboratories, Burlingame, USA)
- Primary antibody (anti-c-Fos Rabbit pAb (Ab-5), Merck)
- Secondary antibody (biotinylated goat anti-rabbit IgG (H+L), Vector Laboratories)
- DAB (3,3'-diaminobenzidine tetrahydrochloride hydrate, 97%, Sigma-Aldrich)
- Nickel(II) chloride Hexahydrate (Sigma-Aldrich)
- Cobalt(II) chloride Hexahydrate (Merck)
- ABC kit (Vectastain®, Vector Laboratories)
- Ethanol
- Xylol
- Rapid mounting medium (Entellan®, Merck)

Table 5 10x Phosphate buffered saline

Substance	Concentration [g/l]	End concentration [mM]
NaCl	80	137
KCl	2	1.47
Na_2HPO_4	18.1	7.81
KH_2PO_4	2.4	2.68
For working solution (1x PBS), 1l of 10x PBS was diluted with 9l ddH_2O and the pH level was adjusted to 7.4 using HCl.		

2.3.3.2 Protocol

The slides were air-dried for one hour before washing them in 0.1% PBST (0.1ml Triton® in 100ml PBS) for ten minutes. To block unspecific antibody binding, a two hour incubation in blocking solution (1.5% in 0.3% PBST) was conducted, followed by another wash in 0.1% PBST (3x10 minutes). Slides were then incubated in 1:5000 primary antibody at 4°C for 36 to 48 hours.

After washing (5x10 minutes), incubation with the secondary antibody (1:400) for 90 minutes and another wash step (3x10 minutes) followed before incubating the slides with the avidin-biotin complex for one hour. For visualization of the antibody binding, slides were incubated in a DAB intensifying solution (PBS with 0.02% H_2O_2, 0.08% NiCl and 0.01% CoCl) for three minutes, followed by a final washing step (3x5 minutes) and dehydration in graded alcohols (50-100%) and xylol. Slices were finally coverslipped with Entellan®.

c-Fos positive cells in the AP and the NTS were evaluated under a light microscope. Four representative and corresponding sections per animal were quantified and averaged to compare c-Fos activation in *ko* and *wt* animals.

2.3.4 Immunohistochemistry for calcitonin receptors

2.3.4.1 Material

- Phosphate buffered saline **(Tab. 5)**
- Triton® X-100 (Sigma-Aldrich)
- Normal donkey serum (Jackson Laboratories)
- Primary antibody (Rabbit anti-CTR, kindly provided by Dr. P. Wookey, Melbourne)
- Secondary antibody (Alexa Fluor® 555 donkey anti-rabbit IgG (H+L), Invitrogen, Basel, Switzerland)
- Citifluor™ (Citifluor Ltd., London, UK)
- Rapid mounting medium (Entellan®, Merck)

2.3.4.2 Protocol

The slides were air-dried and washed as for c-Fos before blocking unspecific antibody binding with 3% normal donkey serum in 0.3% PBST. After washing in PBS (2x10 minutes) and 0.1% PBST (10 minutes), the slides were incubated in 1:1000 primary antibody at 4°C for 36 to 48 hours.

The antibody was removed by washing in PBS (2x10 minutes) and PBST (10 minutes) previous to the incubation in 1:222 secondary antibody for 80 minutes. After the final wash in PBST (10 minutes) and PBS (2x10 minutes), the slices were covered with citifluor and the coverslips fixed with Entellan®.

2.3.4.3 Quantitative analysis

The AP of CTR stained sections was scanned with the confocal laser microscope as described in 2.2.5. The settings were slightly changed for emission detection, as the spectral range of DiI and Alexa 555 are not identical **(Fig. 8)**. Emission was detected between 580 and 650nm; gain and offset were also adjusted manually. Image stacks contained 23 single images with a thickness of 0.8µm, i.e. a total of 18.4µm.

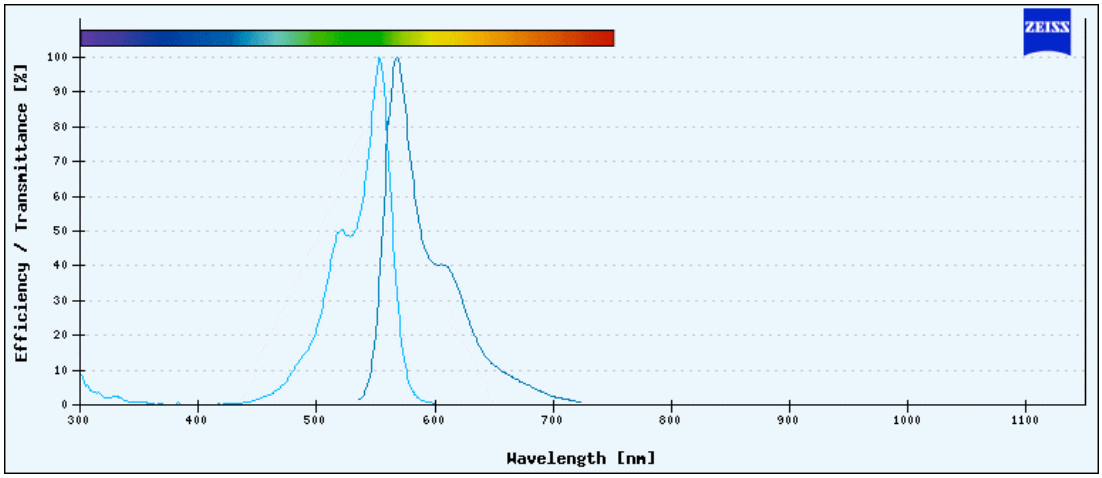

Figure 8 Spectral range of Alexa 555 (adapted from Zeiss Co.)

Light blue = excitation (553nm); dark blue = emission (568nm) of Alexa 555

The stacks were also three-dimensionally reconstructed and analyzed with Imaris 6.4.0 (Bitplane, Zurich, Switzerland). The surface application was used to create an artificial solid object based on gray value range and manual thresholding **(Fig. 9)**. The total volume of all stained objects ("receptor density") in a standardized volume of the AP ($0.184x10^{-3}mm^3$) was calculated for four sections per animal and averaged to compare CTR expression between *ko* and *wt* animals.

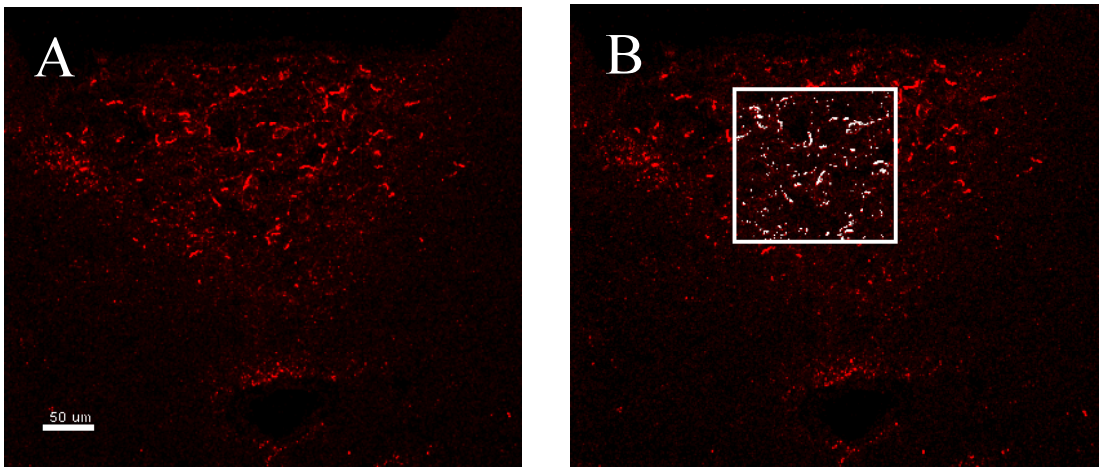

Figure 9 Confocal image stacks of the area postrema after immunohistochemical processing for calcitonin receptors

A Representative three-dimensional reconstruction of confocal image stacks

B Quantification area containing the artificial surface corresponding to CTR density (white box)

2.4 Genotyping

Because all animals used in the present study were the offspring of heterozygous breeding pairs, the genotype was not known at birth. Therefore, biopsies had to be taken in order to extract the DNA, amplify it by PCR and analyze by electrophoresis. Mouse pups were marked by toe amputation on postnatal day 6 or 7. Toes were clipped with a scalpel, collected in labeled 1.5ml Eppendorf tubes and stored at -20°C until analysis.

2.4.1 DNA extraction

2.4.1.1 Material

- Thermal shaker
- Solubilization buffer **(Tab. 10)**
- Proteinase K (Promega Co, Madison, USA)
- Tail salt solution **(Tab. 11)**
- Isopropanol 60%
- Ethanol 70%
- Tris-EDTA buffer **(Tab. 12)**

Table 6 Solubilization buffer (50ml)

Substance	Stock concentration	Amount [g]	Volume [ml]	End concentration [M]
SDS	10 %	0.5	5	1 %
Sodium acetate	3M	1.23	5	0.3M
EDTA	50mM	0.019	1	1mM
Tris-HCl (pH 6.8)	1M	0.061	0.5	10mM
Fill up to 50 ml with aqua dest				

Table 7 Tail salt solution (50ml)

Substance	Concentration [g/50ml]	End concentration [M]
NaCl	12.3	4.21
KCl	2.3	0.63
Fill up to 45 ml with Tris-HCl (10mM), adjust pH to 8.0, fill up to 50 ml		

Table 8 TE buffer (100ml)

Substance	Stock concentration	Amount [g]	Volume [ml]	End concentration [M]
Tris-HCl (pH 8.0)	1M	0.012	0.1	1mM
EDTA	50mM	0.037	2	1mM

2.4.1.2 Protocol

First, 500µl of solubilization buffer and 50µl proteinase K were added to the specimens before incubating them for 30 minutes at 55°C with 950 rpm on a thermal shaker. This step served the lysis of cells and the degradation of DNA-associated proteins. For the precipitation of proteins, 200µl of tail salt solution were added for another incubation with the same parameters. The tubes were centrifuged for 10 minutes at 4°C with 13000rpm and the supernatant was transferred into new Eppendorf tubes. The DNA was precipitated by mixing the supernatant with 500µl of 60% isopropanol, followed by centrifugation for 30 minutes at 4°C with 15000rpm. After decanting the supernatant, the pellet was washed with 500µl ice-

cold 70% ethanol and centrifuged again for 15 minutes at 4°C with 13000rpm. The supernatant was carefully removed before the pellet was air-dried for about 20 minutes. Finally, the pellet was resuspended overnight at room temperature with 100µl of TE buffer. Alternatively, it was dissolved by an incubation for 2 hours at 55°C with 400rpm on the thermal shaker.

2.4.2 DNA amplification

2.4.2.1 Materials

- PCR thermocycler
- ddH_2O
- Green PCR buffer (Promega Co., Madison, USA)
- $MgCl_2$ (Promega Co.)
- dNTP's (Promega Co.)
- Primer Nr. 206 *(ko)*
- Primer Nr. 207 *(ko)*
- Primer Nr. 208 *(wt)*
- Primer Nr. 209 *(wt)*

*see **Tab. 13** for genotype-specific primers*

- Go-Taq® Flexi DNA Polymerase (Promega Co.)
- DNA template

2.4.2.2 Protocol

All substances of the mastermix **(Tab. 14)** were pipetted into a 1.5ml Eppendorf tube, which had been kept on ice. The mix was vortexed and quickly centrifuged at 4°C before 24µl per sample were transferred into sterile 200µl tubes. 1µl of the genomic DNA template to analyze was added to a total volume of 25µl. The tubes were placed in a PCR thermocycler with the following program **(Tab. 15)**: denaturation at 94°C for one minute, followed by 10 cycles of melting at 92°C for 30s, annealing at 65°C for 30s and synthesis at 72°C for 30s; followed by 25 cycles of melting at 92°C, annealing at 62°C for 30s and synthesis at 72°C for 30s; followed by a final extension step at 72°C for 5 minutes. The first 10 cycles served as a touch down to avoid unspecific annealing and therefore unspecific DNA amplification. Samples were kept at 4°C until separation.

Table 9 Primers

Primer	Sequence (5' – 3')	Length [mer]	Tm [°C]	Location	Product size [bp]
206	CTTGGGTGGAGAGGCTATTC	20	58.7°C/57.5	Chromosome 6	200
207	CACAGCTGCGCAAGGAAC	18	61.8°C/57.1		
208	GTAGCAACCCTCAGATGGAC	20	57.2°C/57.5	Chromosome 6	107
209	GAGGACTGGACCAAGGTTGT	20	59.0°C/57.5		

Table 10 Mastermix

Substance	Volume [µl]			Concentration
	1	5	10	
ddH_2O	14.375	71.875	143.75	
Green PCR-Buffer (5x)	5.0	25	50	
$MgCl_2$ 25 mM	2.0	10	20	
dNTP's 2.5 mM each	0.5	2.5	5	
Primer Nr. 206 ko	0.5	2.5	5	10 µm
Primer Nr. 207 ko	0.5	2.5	5	10 µm
Primer Nr. 208 wt	0.5	2.5	5	10 µm
Primer Nr. 209 wt	0.5	2.5	5	10 µm
Go-Taq Flexi Polymerase 5u/µl	0.125	0.625	1.25	0.625 u

Table 11 PCR conditions

Cycles	Time	Temperature	Process step
1	1’	94°C	Start
10	30’’	92°C	Melting
	30’’	65°C	Annealing
	30’’	72°C	Synthesis
25	30”	92°C	Melting
	30”	62°C	Annealing
	30”	72°C	Synthesis
1	5’	72°C	Synthesis
	∞	4°C	Hold

2.4.3 DNA separation

2.4.3.1 Material

- Agarose (#820723, MP Biomedicals, Inc., Solon, Ohio, USA)
- Ethidiumbromide
- DNA ladder (100bp, Fermentas International Inc., Canada)
- TAE buffer **(Tab. 16)**
- Electrophoresis chamber

Table 12 50x TAE buffer

Substance	Concentration [g/l]	End concentration [M]
EDTA	18.61	0.05
Tris-HCL pH 8.0	242	2
Acetic acid	57.1ml	2
Working solution is 1x TAE		

2.4.3.2 Protocol

In a microwave, 2g of agarose were heated in 100ml 1x TAE buffer until completely dissolved. The solution was left to cool for a few minutes before 2µl of ethidium bromide were added and mixed in carefully without creating bubbles. Ethidiumbromide intercalates with the DNA and fluoresces when exposed to UV light; for these reasons it is used to visualize PCR products in the agarose gel.

The gel was poured into the electrophoresis chamber and before it had entirely cooled down, the comb was inserted. If any air bubbles had been created, they were removed with a pipette tip. The chamber was filled with 1x TAE buffer until the gel was covered with 3 to 5mm of the buffer solution.

After the comb had been removed, 12µl of each sample were loaded besides a molecular DNA weight marker (100bp DNA ladder) for size estimation. Furthermore, representative samples and mastermix without DNA template were loaded as positive and negative controls. Electrophoresis was run with a voltage of 140V for about 40 minutes; afterwards the gel was exposed to UV light for documentation of the amplicons **(Fig. 10)**. The sizes of amplicons were expected as follows for the different genotypes:

Table 13 Expected bands

Genotype	Primers	Amplicon size
-/- *knockout*	206/207	200bp
	208/209	No product
+/- *heterozygous*	206/207	200bp
	208/209	107bp
+/+ *wildtype*	206/207	No product
	208/209	107bp

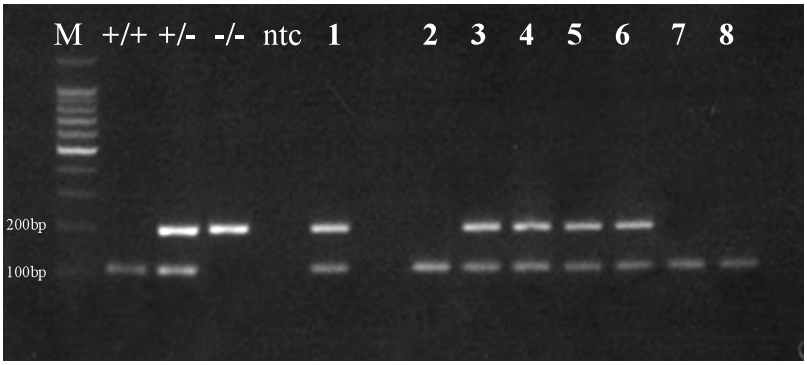

Figure 10 Agarose gel after electrophoresis showing the amplicons

M = molecular DNA marker; +/+ = wildtype; +/- = heterozygous; -/- = knockout; ntc = no template control; 1-8 = test specimens: 1, 3, 4, 5, 6 = heterozygous; 2, 7, 8 = wildtype

2.5 Statistical analysis

All data are presented as means ± SEM. Statistical significance was determined by parametric t-test of data with normal distribution (Kolmogorov-Smirnov normality test) using Prism Version 5.0a for Mac OS X (GraphPad Software Inc., San Diego, CA, USA). A p-value < 0.05 was considered statistically significant.

3 Results

3.1 Neurotrophic effects of amylin

3.1.1 Fiber density in the NTS on P10, P14 and P60

In a previous study, we found a significantly reduced fiber density in the NTS of P10 $IAPP^{-/-}$ mouse pups compared to $IAPP^{+/+}$ littermates (**Fig. 1**). Interestingly, there was only a tendency towards a reduction in P14 $IAPP^{-/-}$ mice, which did not reach statistical significance compared to their wildtype littermate controls (results not shown). Because of the relatively low number of animals with the appropriate genotype in this experiment, male and female littermates had been combined to final group sizes of 5 and 6 for $IAPP^{-/-}$ and $IAPP^{+/+}$ mice, respectively.

To eliminate a possible influence of gender differences on the development of AP to NTS projections, we excluded all female mice from the previous study and included additional male animals in the present study. This resulted in a total number of six male P14 $IAPP^{-/-}$ and five male $IAPP^{+/+}$ mice, respectively. The results were comparable to our previous data; in other words, we did not observe a significant difference in total fiber length between $IAPP^{-/-}$ (7707 ± 1489) and $IAPP^{+/+}$ mice (11800 ± 3456); the P value of $p = 0.3$ was similar as before. When comparing the male wildtype mice between P10 and P14, total fiber length differed significantly between P10 $IAPP^{+/+}$ and P14 $IAPP^{+/+}$ male mouse pups, supporting the hypothesis of neural remodeling processes during this time window (**Fig. 1**). Hence, the lack of significant difference in total fiber length between P14 $IAPP^{-/-}$ and $IAPP^{+/+}$ mice was mainly due to a marked reduction in fiber density in the wildtype controls. The fiber density of $IAPP^{-/-}$ mice however did not significantly change from P10 to P14 and P60.

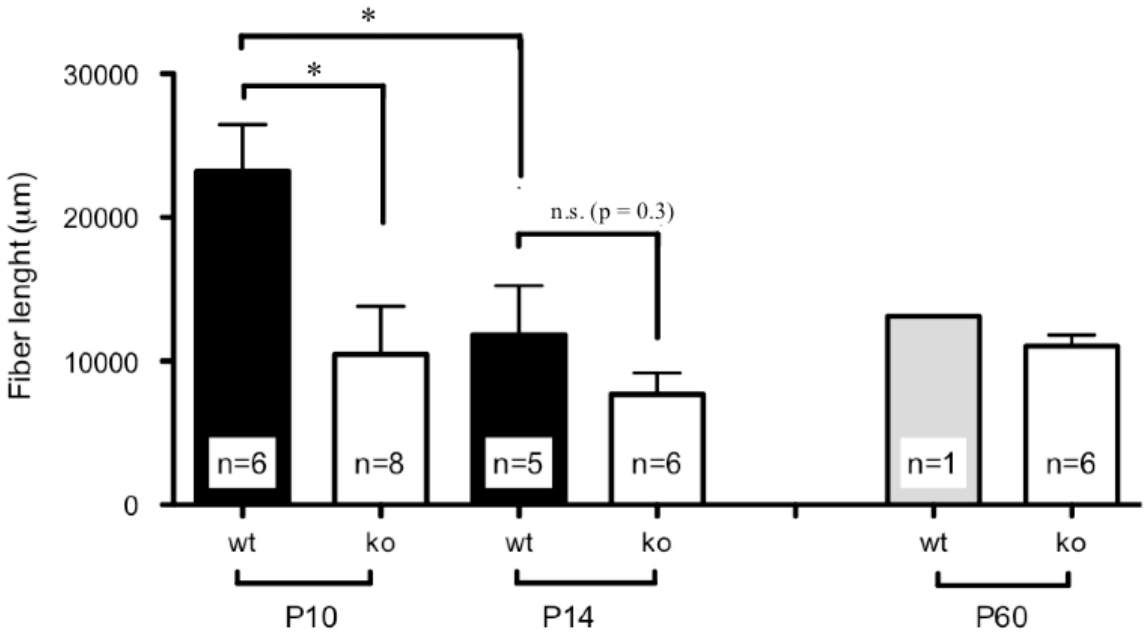

Figure 11 Total fiber length in the NTS of male P10, P14 and P60 IAPP$^{+/+}$ and IAPP$^{-/-}$ mice (P10 data from A. Hermann)

The total fiber length in a volume of 3.4x 10^{-3}mm^3 on P10 was significantly lower in IAPP$^{-/-}$ mice (10460 ± 3341) compared to wildtype littermates (23160 ± 3265) ($p < 0.05$); there was also a significant decrease in wildtype IAPP$^{+/+}$ males between P10 and P14 ($p < 0.05$). Fiber length in IAPP$^{-/-}$ mice on P60 was similar to IAPP$^{+/+}$ animals but the data are preliminary (n=1 in the wildtype controls). In IAPP$^{-/-}$ mice, the fiber density did not significantly change between P10, P14 and P60.All data are expressed as mean ±SEM; *$p < 0.05$; n.s. = not significant

To investigate a possible impact of amylin deficiency on the AP/NTS neuroanatomy of adult mice, tracing studies with P60 mice were conducted. Due to temporary breeding problems, the number of animals that were analyzed (i.e. after the exclusion of animals with unsuccessful implantations) was relatively low. P60 IAPP$^{-/-}$ (11040 ± 750, n=6) animals showed a fiber density similar to the only P60 IAPP$^{+/+}$ animal (13099) included in the experiment. Fiber density was also similar to P14 IAPP$^{+/+}$ (11800 ± 3456, n=5) mice. Further investigation is required before definite conclusions can be drawn about the consequences of amylin deficiency for the neuroanatomy of adult mice.

Typical examples for the density of projections from the AP to the NTS in IAPP$^{-/-}$ and IAPP$^{+/+}$ mice of different ages are shown in **Figures 2**, **3** and **4**.

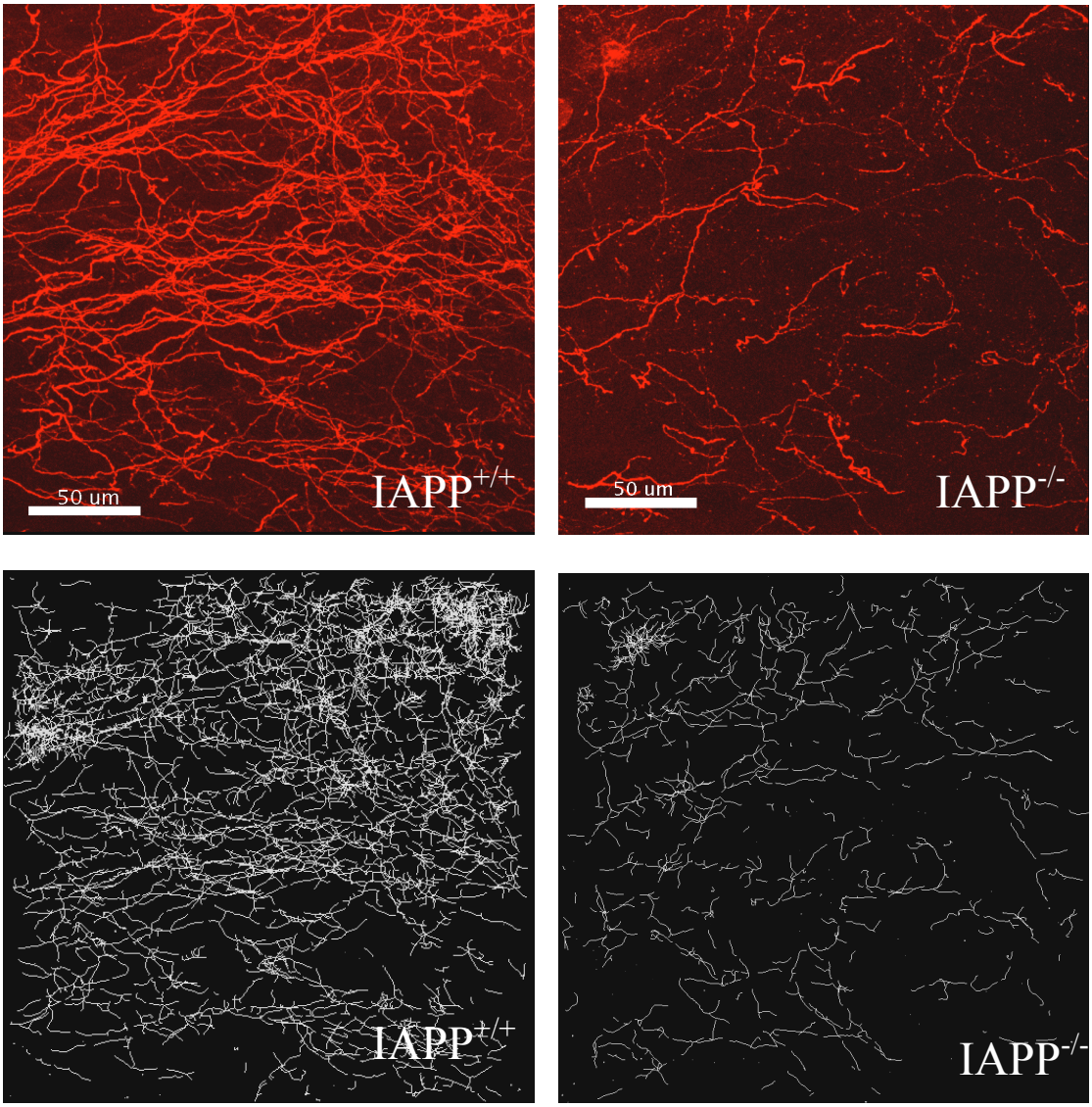

Figure 12 Representative confocal image stacks and created fiber skeleton of the NTS in P10 mice (images from A. Hermann)

A+B Three-dimensionally reconstructed confocal image stacks of the NTS region of male P10 IAPP$^{+/+}$ and IAPP$^{-/-}$ littermates

C+D Skeletonized fibers corresponding to the confocal images A+B and used for the quantification of total fiber length

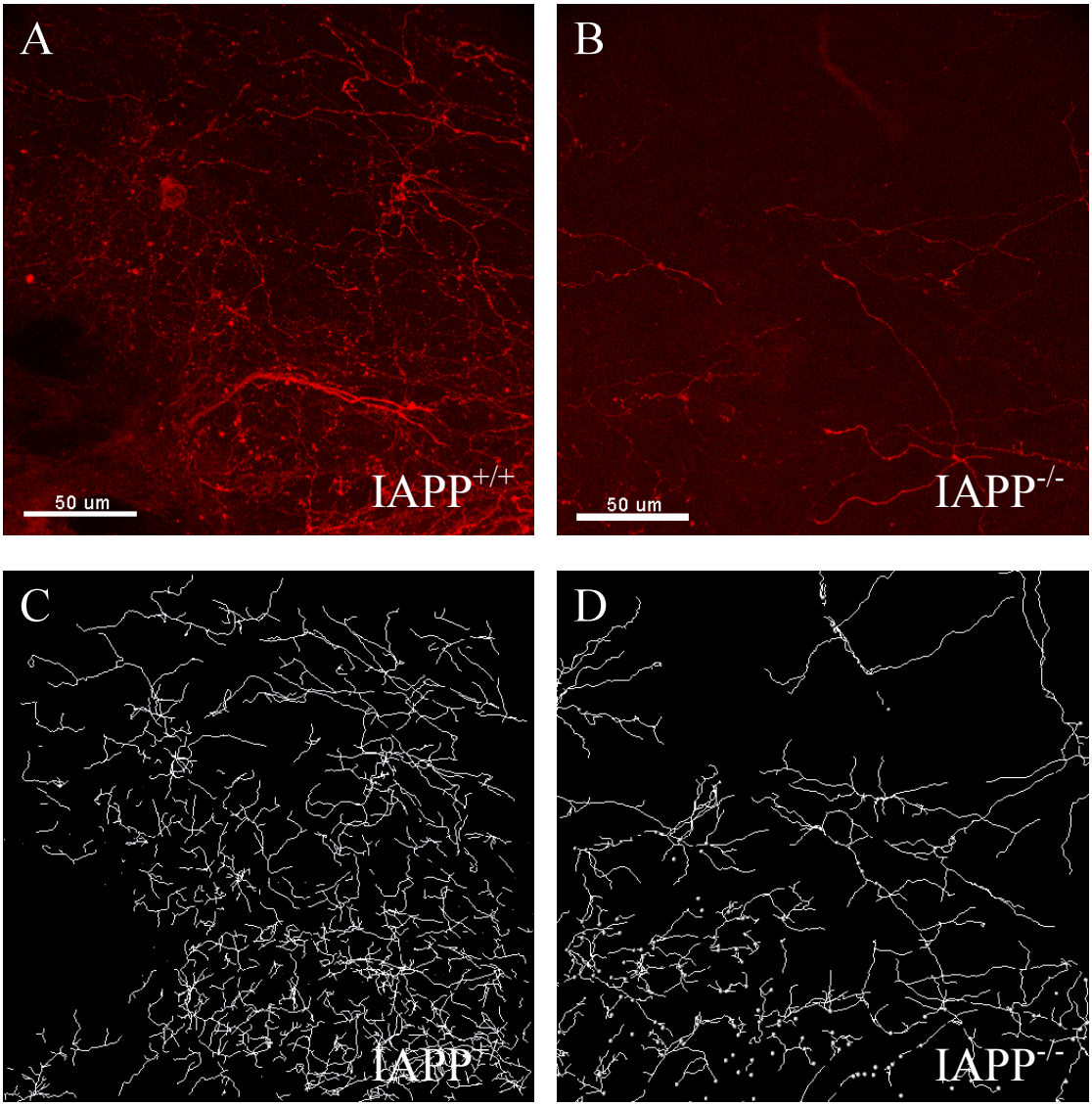

Figure 13 Representative confocal image stacks and created fiber skeleton of the NTS in P14 mice

A+B Three-dimensionally reconstructed confocal image stacks of the NTS region of male P14 IAPP$^{+/+}$ and IAPP$^{-/-}$ littermates

C+D Skeletonized fibers corresponding to the confocal images A+B and used for the quantification of total fiber length

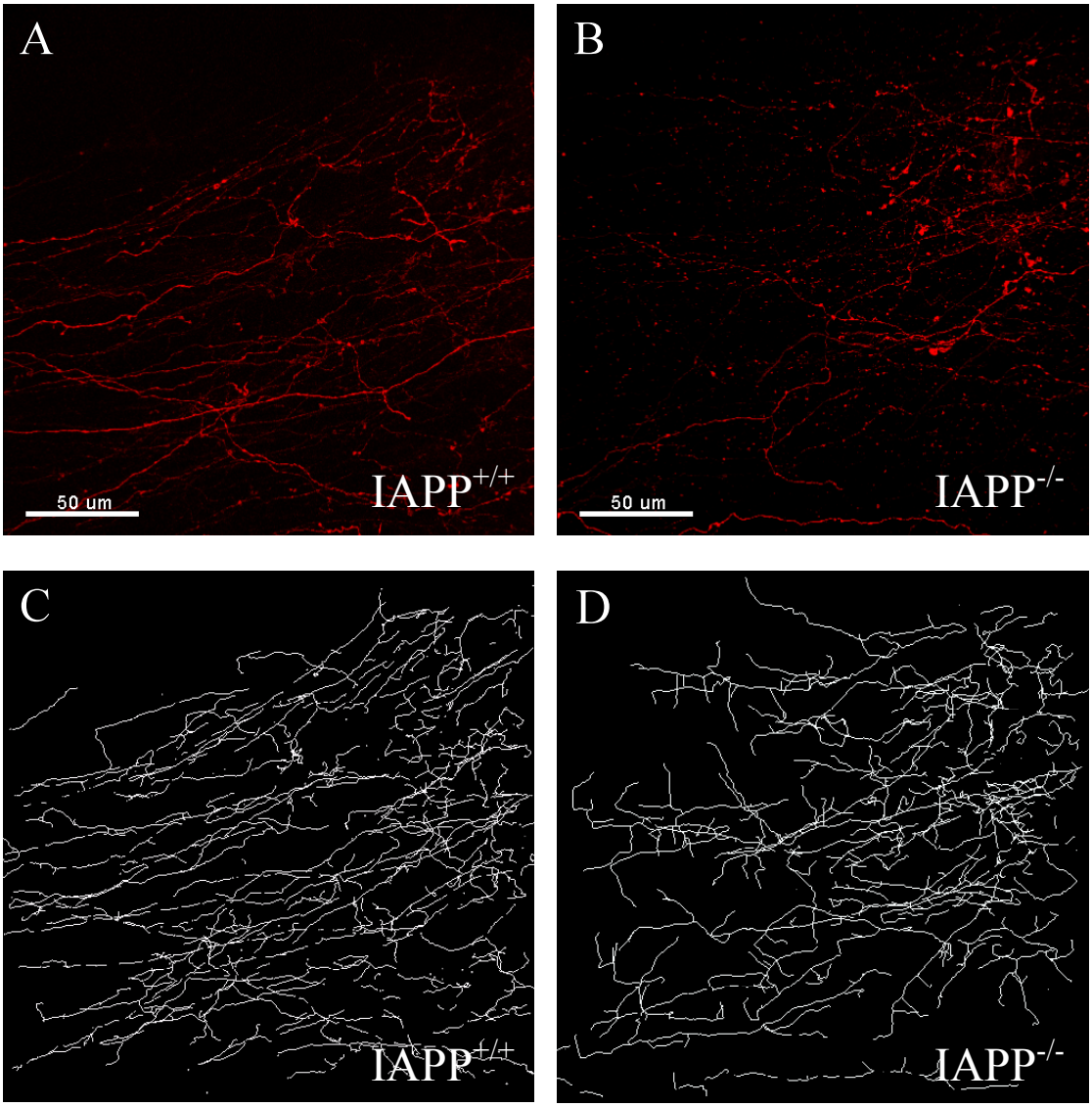

Figure 14 (preliminary data) Representative confocal image stacks and created fiber skeleton of the NTS in P60 mice

A+B Three-dimensionally reconstructed confocal image stacks of the NTS region of male P60 IAPP$^{+/+}$ and IAPP$^{-/-}$ littermates

C+D Skeletonized fibers corresponding to the confocal images A+B and used for the quantification of total fiber length

3.2 c-Fos expression and calcitonin receptor density in the AP

3.2.1 c-Fos expression in the AP/NTS region of adult mice

To investigate signal transduction from the AP to the NTS in adult IAPP$^{+/+}$ and IAPP$^{-/-}$ mice, an immunohistochemical study for amylin-induced c-Fos expression was performed. There was no significant difference in the number of c-Fos positive cells 120 min after amylin injection between male P60 IAPP$^{+/+}$ (n=3) and IAPP$^{-/-}$ (n=5) mice either in the AP (wt: 70 ± 7; ko: 57 ± 4) or in the NTS (wt: 38 ± 1; ko: 38 ± 3) (**Fig. 5 + 6)**.

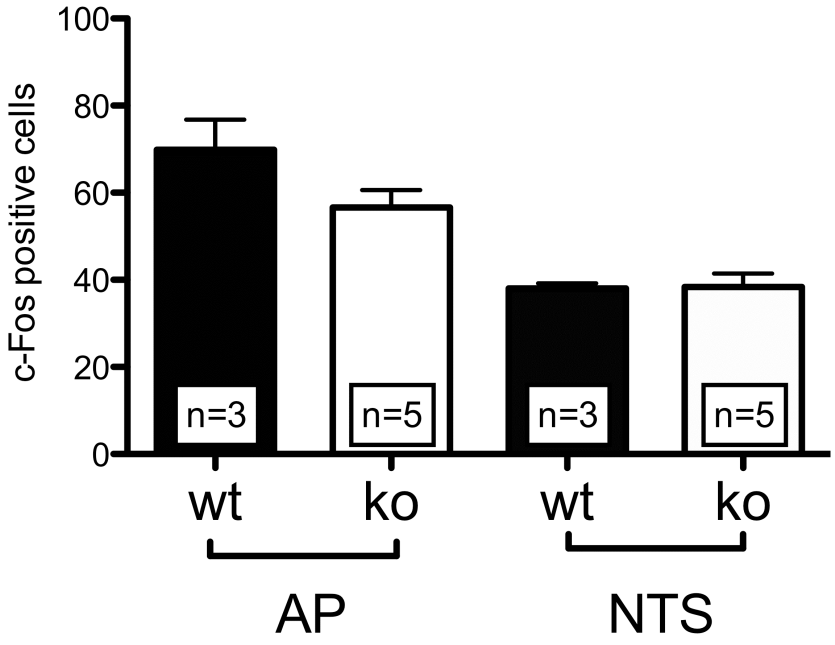

Figure 15 Number of c-Fos expressing cells in the AP and NTS of male P60 IAPP$^{+/+}$ and IAPP$^{-/-}$ mice 120 min after amylin injection (50µg/kg SC)

There was no significant difference in the number of c-Fos positive cells in either the AP or the NTS of IAPP$^{+/+}$ and IAPP$^{-/-}$ mice. All data are expressed as mean ±SEM

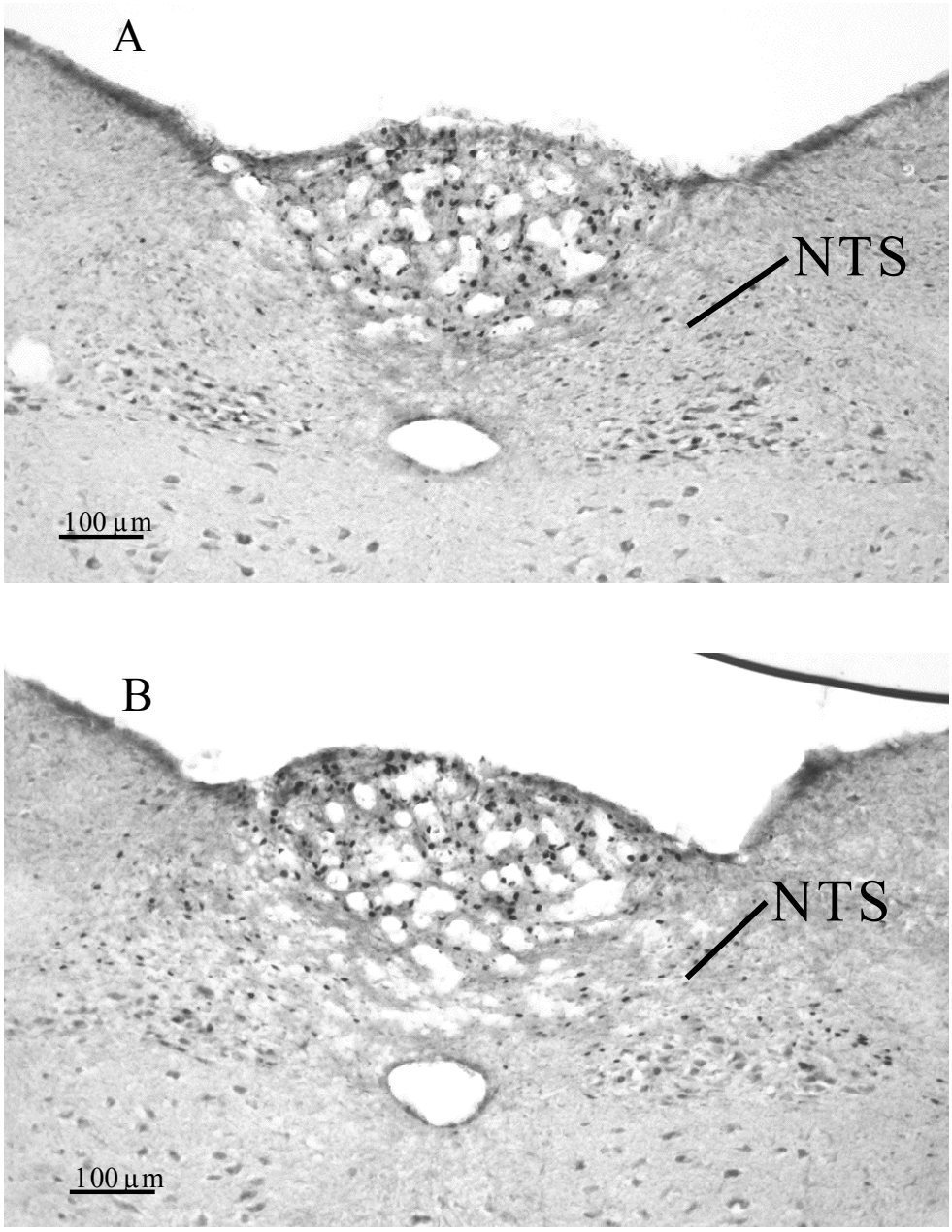

Figure 16 c-Fos expression in the AP and NTS of male P60 IAPP$^{+/+}$ (A) and IAPP$^{-/-}$ mice (B) after amylin injection

NTS = nucleus of the solitary tract

3.2.2 Calcitonin receptor density in the AP of adult mice

The density of calcitonin receptors in the AP of female P60 IAPP$^{+/+}$ (n=4) and IAPP$^{-/-}$ (n=3) mice was determined by immunohistochemistry with antibodies specific against the CTR protein. IAPP$^{-/-}$ animals expressed a higher density of CTR in the AP than IAPP$^{+/+}$ animals (6201 ± 1746 vs. 2610 ± 707, respectively), however the difference failed to reach statistical significance (p = 0.086) (**Fig. 7 + 8**).

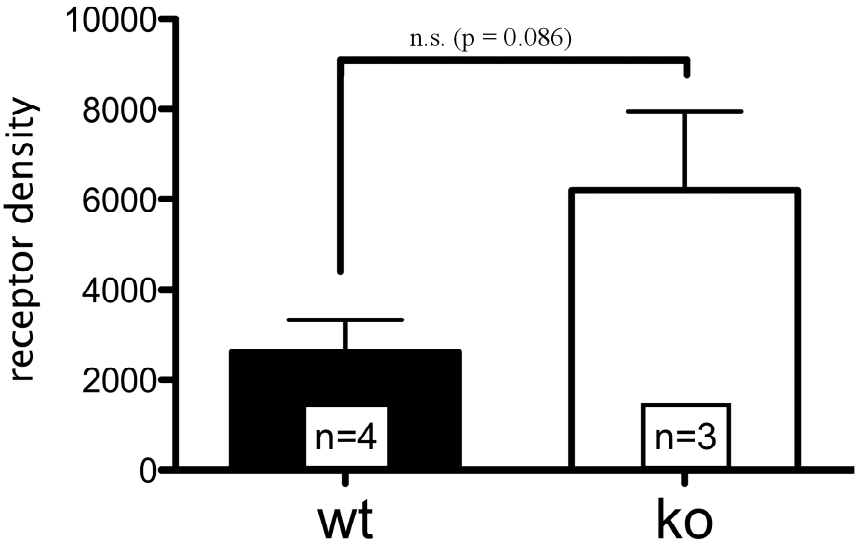

Figure 17 CTR density in the AP of female P60 IAPP$^{+/+}$ and IAPP$^{-/-}$ mice

CTR expression in the AP was higher in IAPP-/- animals, but the difference was not statistically significant. All data are expressed as mean ±SEM; n.s. = not significant

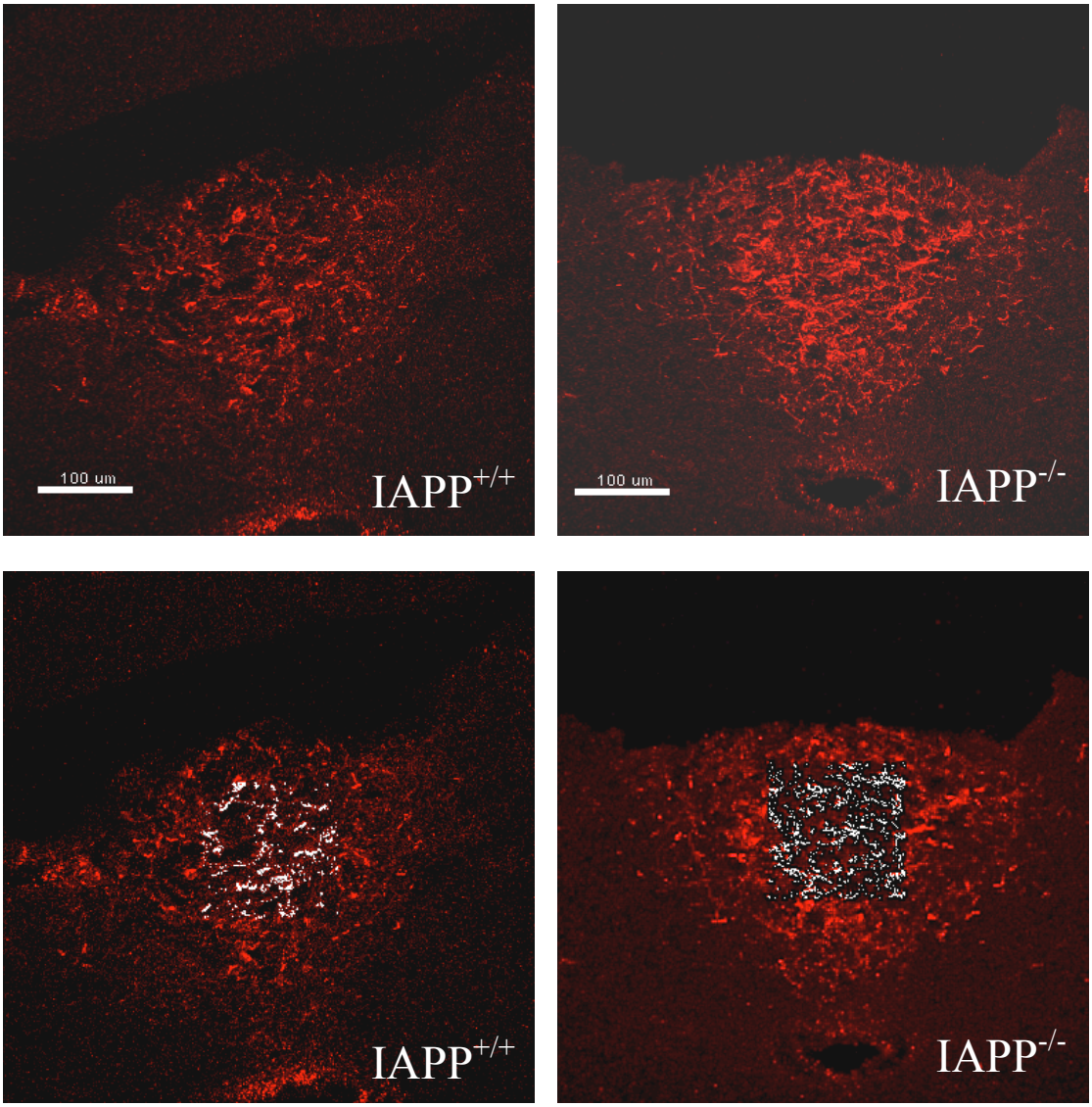

Figure 18 Representative confocal image stacks of the AP and created artificial surfaces

A+B Three-dimensionally reconstructed confocal image stacks of the AP of female P60 IAPP$^{+/+}$ and IAPP$^{-/-}$ mice

C+D Artificial surface corresponding to the confocal images A+B and used for the quantification of CTR density

3.3 Neurotrophic effects of leptin in the AP

3.3.1 Fiber density in the NTS on P14

For DiI tracing studies in leptin-deficient *ob/ob* mice, Dr. S. Bouret kindly provided us with perfused brains of leptin-deficient *ob/ob* and control mice. The experiments were conducted with male wildtype (n=6) and *ob/ob* (n=7) littermates on postnatal day 14 (P14).

The fiber density in the NTS (expressed as total fiber length in a volume of 3.4 x $10^{-3}mm^3$) was significantly reduced in P14 *ob/ob* mice compared to their wildtype littermates. The total fiber length was 14910 ± 1574µm in wildtype mouse pups versus 9833 ± 1040µm in *ob/ob* animals ($p<0.05$) (**Fig. 9**).

A typical example of the reduced density of projections from the AP to the NTS in *ob/ob* mice is shown in **Figure 10**.

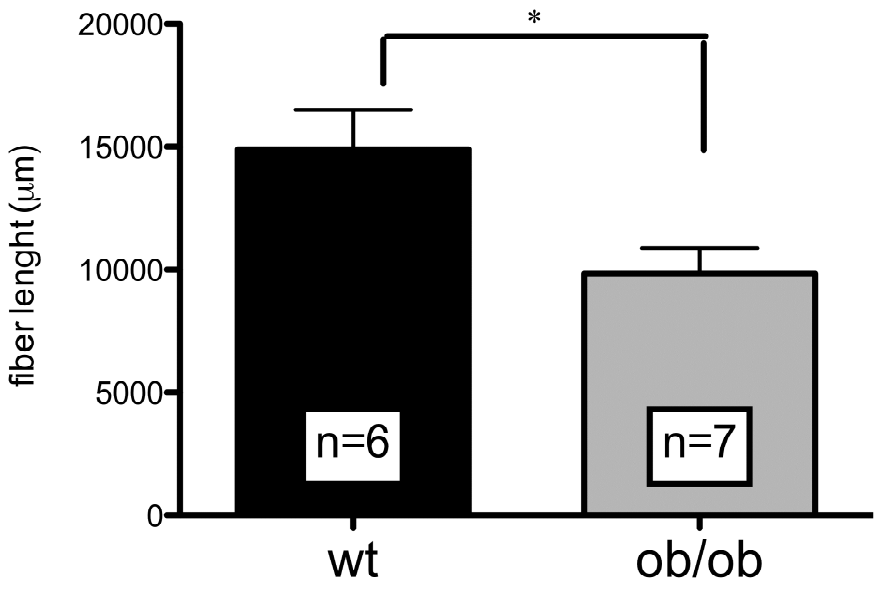

Figure 19 Total fiber length in the NTS of male P14 *ob/ob* and wildtype mouse pups

The total fiber length in a volume of 3.4x $10^{-3}mm^3$ was significantly lower in *ob/ob* mice compared to wildtype littermates. All data are expressed as mean ±SEM: **p<0.05

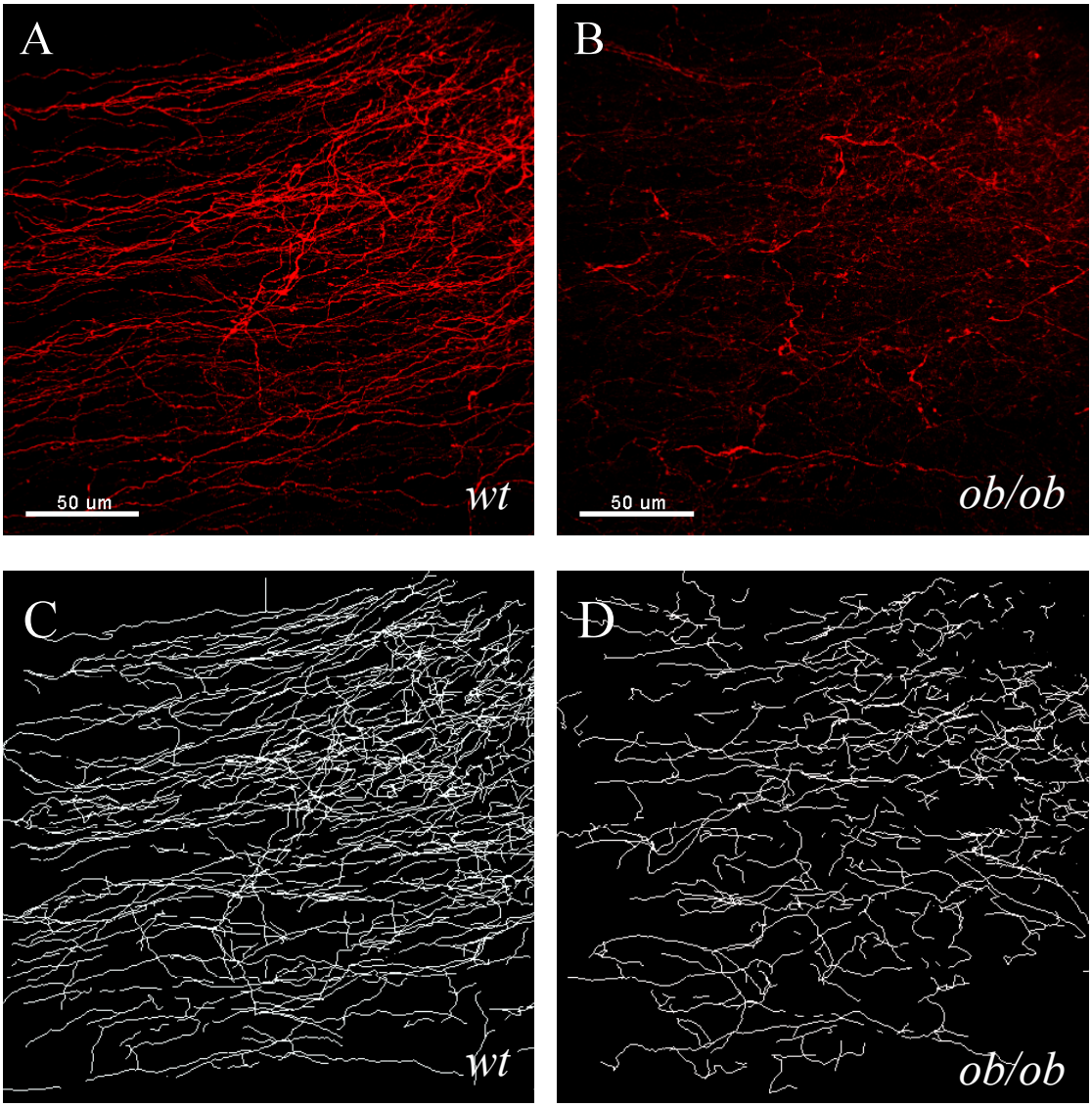

Figure 20 Representative confocal image stacks and created fiber skeleton of the NTS

A+B Three-dimensionally reconstructed confocal image stacks of the NTS region of male P14 wildtype and *ob/ob* littermates

C+D Skeletonized fibers corresponding to the confocal images A+B and used for the quantification of total fiber length

3.3.2 Long projections to other brain regions

The DiI tracer did not only label fibers from the AP to the NTS, but also projections to other brain regions. In all DiI-labeled brains of *ob/ob* and wildtype mice, large bilateral projections emerging ventrolaterally from the NTS were detected (**Fig.11**), which is similar to our previous findings in amylin-deficient $IAPP^{-/-}$ and wildtype $IAPP^{+/+}$ control mice.

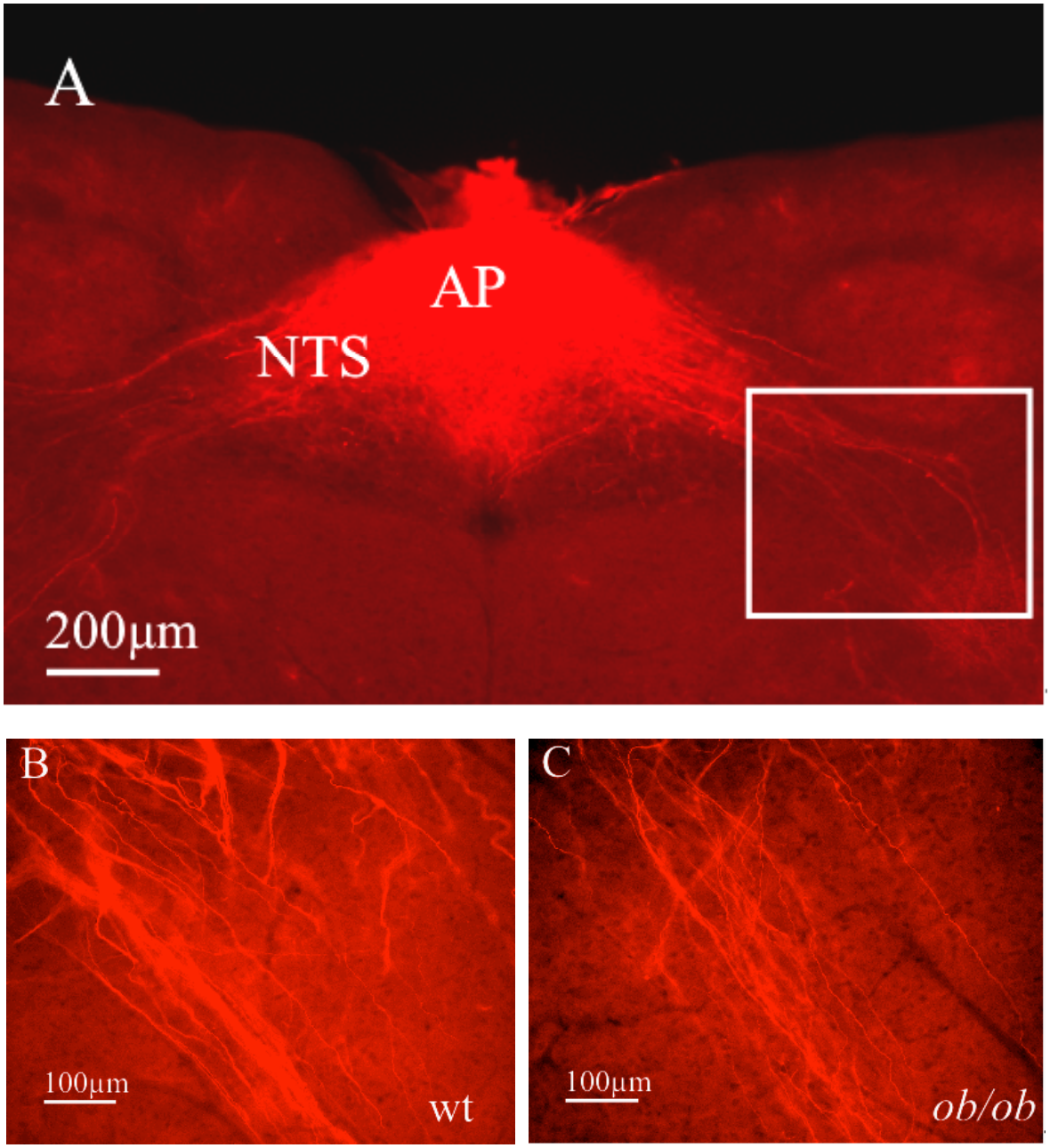

Figure 21 Fluorescence microscopic images of large projections outside the NTS in male P14 *ob/ob* and wildtype mice

A Low magnification of projections emerging ventrolaterally from the NTS (white box = magnification in B + C); *AP = area postrema, NTS = nucleus of the solitary tract*

B+C High magnification of these projections in wt and *ob/ob* littermates

These projections have previously been described in anterograde tracing studies and terminate to some extent in the nucleus ambiguus, before ascending to the parabrachial nucleus (Shapiro and Miselis 1985; van der Kooy and Koda 1983). We evaluated the fiber density of these projections semi-quantitatively with a ranking from 1-3, which revealed a

higher fiber density in *ob/ob* mice compared to wildtypes. Data analysis with the chi-square test for trend showed statistical significance ($p < 0.05$) (**Fig. 12**).

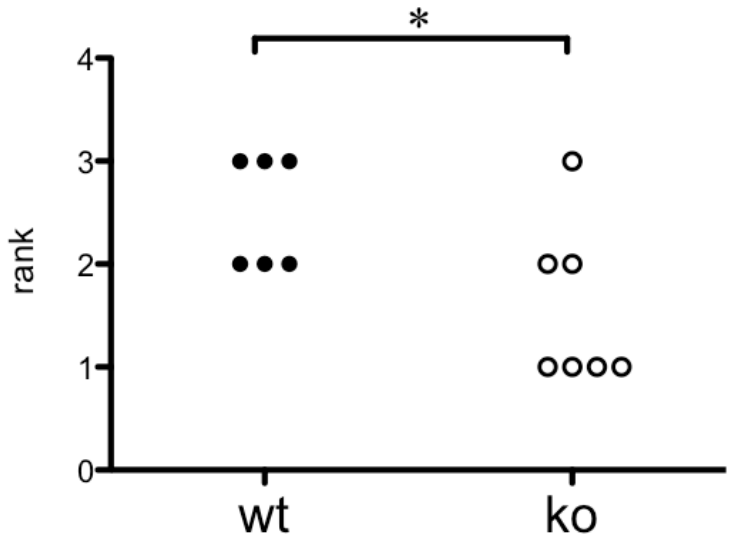

Figure 22 Semi-quantitative analysis of projections outside the NTS in male P14 ob/ob mice and wildtype littermates

Ob/ob mice showed a tendency towards lower fiber content in a semi-quantitative ranking from 1 to 3. Analyzed by chi-square test for trend; *$p < 0.05$

3.4 Establishment of ARH implantations

It was the aim of the last part of the current study to establish the DiI tracing for the detection of ARH-PVN projections as described by *Bouret et. al*. (Bouret et al. 2004b). Using this approach, first studies were conducted to characterize the influence of amylin deficiency on the development on these neuronal projections. Our experiments showed that a crystal size of 25µm was most appropriate for P14 $IAPP^{+/+}$ and $IAPP^{-/-}$ mice in order to keep the unspecific tracer diffusion restricted to the ARH (**Fig. 13**).

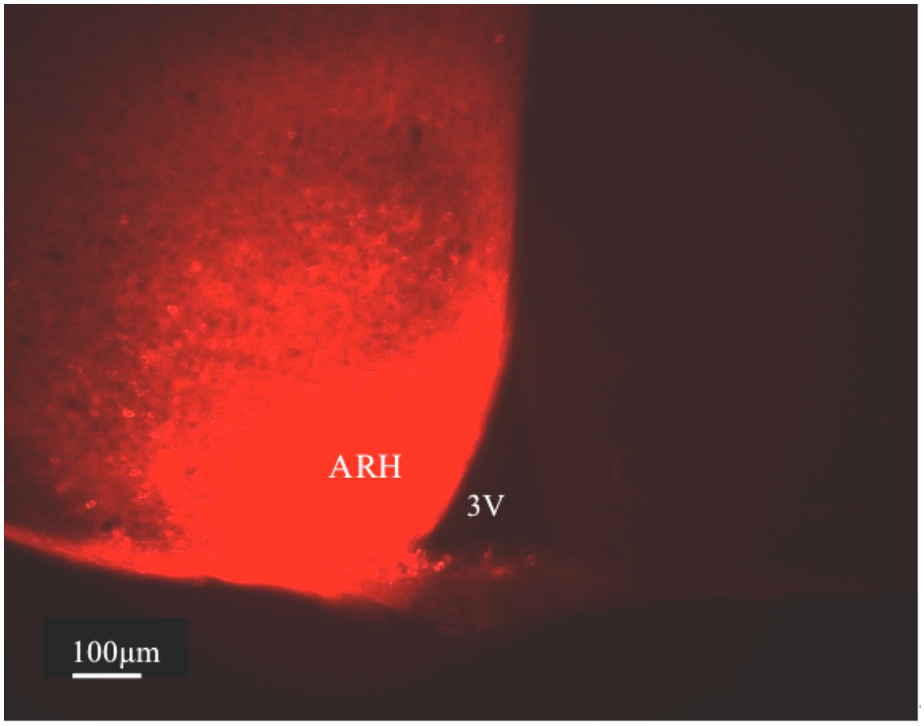

Figure 23 Fluorescence microscopic image of DiI implantation site in the ARH

ARH = arcuate nucleus of the hypothalamus, 3V = third ventricle

Because we first had to establish this method in our laboratory, the number of analyzable slices is not yet sufficient for statistical analysis; nonetheless, it was very interesting to note that male P14 IAPP$^{-/-}$ mice showed a tendency towards a reduction in total fiber length compared to IAPP$^{+/+}$ littermates (**Fig. 14 + 15**), similar to previous observations comparing leptin-deficient *ob/ob* mice and wildtype controls.

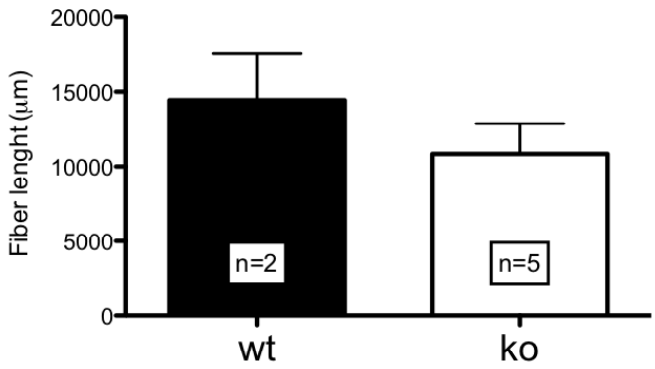

Figure 24 Total fiber length in the PVH of male P14 IAPP$^{-/-}$ and IAPP$^{+/+}$ mouse pups

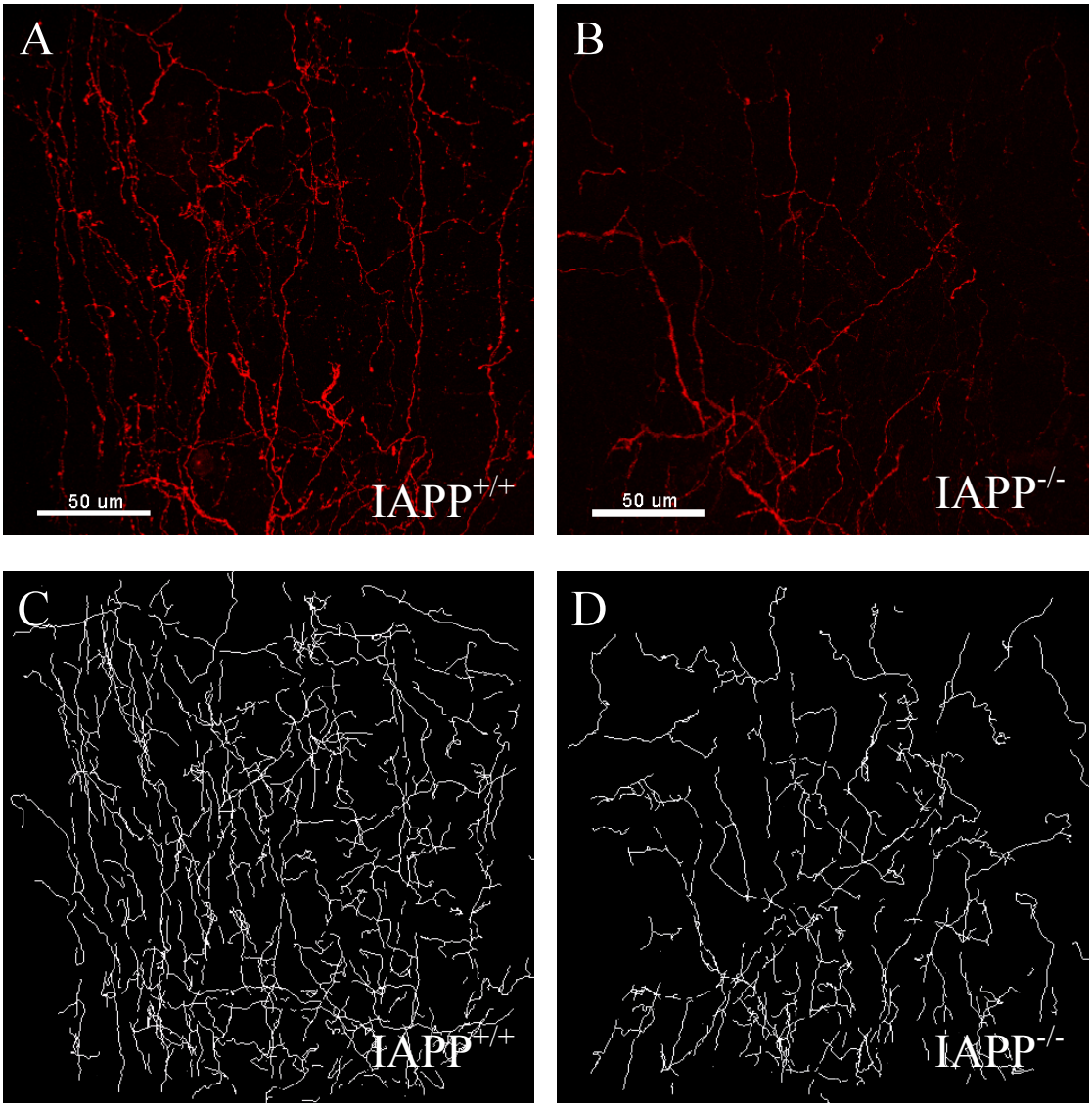

Figure 25 Representative confocal image stacks and created fiber skeleton of the PVH

A+B Three-dimensionally reconstructed confocal image stacks of the PVH region of male P14 IAPP$^{-/-}$ and IAPP$^{+/+}$ littermates

C+D Skeletonized fibers corresponding to the confocal images A+B and used for the quantification of total fiber length

4 Discussion

The aim of the present study was to further characterize the neurotrophic effects of amylin and leptin on the development of neuronal projections in the CNS. The neurotrophic effects of leptin on projections from the arcuate nucleus of the hypothalamus (ARH) to other hypothalamic regions, namely the paraventricular nucleus (PVH), the lateral hypothalamic area (LHA) and the dorsomedial nucleus (DMH), have recently been demonstrated by axonal projection labeling (Bouret et al. 2004b). Our hypothesis that amylin has similar effects on the development of projections from the area postrema (AP) to the nucleus of the solitary tract (NTS) was encouraged by studies demonstrating trophic effects of amylin on the kidney (Harris et al. 1997; Wookey et al. 1998), pancreas (Karlsson and Sandler 2001) and bone tissue (Cornish et al. 2001; Cornish et al. 1995).

Our group investigated this hypothesis in a previous study by using and adapting the DiI tracing method described by *Bouret et al.* (2004). We found a reduced fiber density in $IAPP^{-/-}$ compared to $IAPP^{+/+}$ mouse pups on P10, which provided strong evidence of a neurotrophic effect of amylin on AP-NTS projections. Fibers on P14 were also reduced, but not statistically significant, and there was an overall tendency towards lower fiber density on P14 compared to P10. However, in our previous study only a low number of animals were available, including males and females, which did not permit gender-specific data analysis. For this reason, we collected additional data of male P14 pups in the present study, which allowed us to analyze and compare the data specifically in male mice.

Overall and consistent with the previous preliminary data, our results indicate that P14 male mice of both genotypes have a similar fiber density in respect to their AP to NTS projections. We still observed a tendency towards lower fiber density in male P14 $IAPP^{-/-}$ compared to $IAPP^{+/+}$ mice, but the effect was not significant. Hence, the clear and significant difference in fiber density between $IAPP^{-/-}$ and $IAPP^{+/+}$ P10 mice seems to wane, mainly because of a reduction of fiber density in the wildtype mice between days P10 and P14. In other words, the reduction of fibers in male $IAPP^{+/+}$ mice from P10 to P14, which was observed in the first study, reached statistical significance due to the additional data. This provides additional evidence for regressive neuronal remodeling processes in the AP-NTS projections of $IAPP^{+/+}$ mice between P10 and P14. Although our previous combined data for both genders yielded a similar outcome for P14 animals, it remains to be investigated specifically whether female mice display generally lower AP-NTS fiber densities. This is at

least suggested by our previous gender-specific data of P10 mice, although inclusion of more animals is required to further support this assumption.

Feeding studies in adult IAPP$^{+/+}$ and IAPP$^{-/-}$ mice showed no difference in basal food intake between genotypes (Gebre-Medhin et al. 1998a). In addition, recent studies from our group showed a similar sensitivity of IAPP$^{+/+}$ and IAPP$^{-/-}$ animals to the eating inhibitory effects of exogenous amylin (Theis, 2009). These data indicate that despite the neuroanatomical deficits in early postnatal IAPP$^{-/-}$ mice, this defect may not result in functional insensitivity to the effect of amylin.

We were therefore interested in the consequences of amylin deficiency on the neuroanatomy of adult mice. This was investigated using the same axonal labeling approach as for mouse pups. Furthermore, we wanted to determine a possible impact of amylin deficiency and its impact on brain neuroanatomy on signal transduction in the AP/NTS region of adult mice using c-Fos expression as a neuronal activation marker, and on calcitonin receptor density in the AP.

Our tracing studies showed that there was no significant change in fiber density of IAPP$^{-/-}$ animals from P10 and P14 to P60. A similar comparison for IAPP$^{+/+}$ mice was not yet possible because the group of adult IAPP$^{+/+}$ mice only comprised one animal due to temporary breeding problems; hence, these data have to be considered preliminary. Under the assumption that this animal is representative for P60 male IAPP$^{+/+}$ mice in general, we would have to conclude that there is no difference in fiber density between adult IAPP$^{-/-}$ and IAPP$^{+/+}$ animals on P60. This would in principle be consistent with the data on P14. Additionally, there was no indication for a further decrease in fiber density for AP to NTS projections in male IAPP$^{+/+}$ mice between P14 and P60.

The density of CTR was higher in the AP of IAPP$^{-/-}$ mice compared to wildtype controls; the difference was not yet significant but very close to statistical significance. The non-significant outcome has to be interpreted cautiously based on the current group size. An increased CTR density in IAPP$^{-/-}$ mice is in principle consistent with the assumption that hormone receptors show a compensatory upregulation in hormone-deficient animal models. This phenomenon has been shown in the brains of *ob/ob* mice, which is probably a result of the lack of inhibition by leptin binding to its receptors (Huang et al. 1997). We speculate that a similar mechanism may be responsible for the high density of CTR, as one of the two main components of functional amylin receptors, in the AP of IAPP$^{-/-}$ mice, because autoregulatory

receptor-ligand interactions have already been described for calcitonin receptor-like receptors (Kuwasako et al. 2000).

Finally, we analyzed the signal transduction from the AP to the NTS by c-Fos immunocytochemistry in adult IAPP$^{-/-}$ mice. Consistent with the findings in adult IAPP$^{-/-}$ mice that showed no difference in fiber density compared with wildtype controls, there was no significant difference in the number of c-Fos expressing cells after amylin injection neither in the AP nor in the NTS between IAPP$^{-/-}$ and control mice. We therefore conclude that IAPP$^{-/-}$ mice on P60 are similarly sensitive to the effect of exogenous amylin on neuronal activation in the AP, and that the signal transduction to the NTS as measured by c-Fos immunocytochemistry is not affected by amylin deficiency in adult mice. This is also supported by the study from our group mentioned above, which showed no difference in the sensitivity to the eating inhibitory effect of exogenous amylin between adult IAPP$^{-/-}$ and IAPP$^{+/+}$ mice (Theis, 2009). These same mice had also been used in a parallel study to investigate the c-Fos expression in the AP/NTS region after amylin administration; in that experiment the numbers of amylin-activated cells in the AP and the NTS of IAPP$^{-/-}$ mice was significantly higher compared to IAPP$^{+/+}$ mice. The different outcome between this study and the current finding can most likely be explained by different experimental conditions such as fasting time before amylin treatment and different durations between amylin injection and transcardial perfusion. Furthermore, mice used in the experiment by Theis (2009) were older than P60. It is tempting to speculate that CTR density in the AP might continue to increase after P60, which would explain the increased sensitivity to amylin gauged by c-Fos expression in older IAPP$^{-/-}$ mice. However, neither fiber density nor CTR density have been investigated in IAPP$^{-/-}$ mice older than P60.

Our findings in adult IAPP$^{-/-}$ mice raise questions about the physiological relevance of the reduced fiber density in early postnatal amylin-deficient mouse pups. Although we did not detect significant differences in fiber density of P14 and adult IAPP$^{-/-}$ mice compared to IAPP$^{+/+}$, it remains unknown if the quality of neuronal circuits is affected. Neither the signal transduction from the AP to the NTS nor the eating inhibition after amylin injection was affected by amylin deficiency in adult mice; however, this does not rule out that other functions mediated by the AP or other hormonal systems may be impaired. There are indications supporting the latter hypothesis in the finding that IAPP$^{-/-}$ mice showed differences in body weight gain between weaning and about 4 months of age compared to IAPP$^{+/+}$; of note food intake during this period did not differ significantly between groups (Lutz 2006).

We speculate that the impaired projection development in the hindbrain during early postnatal life in IAPP$^{-/-}$ mice may have a secondary effect on the functional or anatomical maturation of other neuronal circuits in this particular period, leading to a neuronal programming that might persist throughout life. Such effects are not necessarily reflected by AP-NTS fiber densities, but possibly by neuroanatomical or functional deficits in downstream pathways connecting the AP/NTS region to forebrain areas.

Finally, we adapted and established the method of DiI implantation into the ARH in order to investigate ARH-PVH projections. Our data are too preliminary to draw conclusions, although we saw a tendency towards lower fiber density in male P14 IAPP$^{-/-}$ mice compared to IAPP$^{+/+}$ littermates. The analysis of a possible impact of amylin deficiency on the development of ARH projections will be very interesting. A recent study showed an amplification of hypothalamic leptin signaling, detected by c-Fos expression, after amylin administration (Turek et al.), although amylin itself does not activate c-Fos expression in the hypothalamus (Riediger et al. 2004). It will be interesting to see whether, similar to these synergistic neuronal mechanisms, leptin and amylin also interact as developmental neurotrophic factors (see below).

The neurotrophic effect of leptin on the development of projections from the ARH to the PVH had been demonstrated by Bouret et al. (Bouret et al. 2004b). Because our studies had shown a similar effect for amylin on AP-NTS projections, it was of high interest to determine whether leptin may also exert trophic effects on axonal growth in the AP/NTS region, where the leptin receptor is also expressed (Dallaporta et al. 2009); this had never been tested before.

In our study, male *ob/ob* mouse pups in fact showed a significantly reduced fiber density in the NTS compared to wildtype littermates on P14. This result is highly interesting as it further substantiates for a role of the adiposity signal leptin as a developmental signal, which seems to be important for the maturation of pathways involved in the control of energy balance. Based on our findings, a future approach would be the investigation of neuronal projections in leptin and amylin double knock out animals. A recent study led to the suggestion that intrinsic synergistic neuronal signaling pathways for leptin and amylin exist, and that their activation plays a key role in the weight- and fat-reducing effect of combined treatment with amylin and leptin (Turek et al.). It is therefore of high interest whether the neurotrophic actions of amylin and leptin on AP-NTS projections also show some sort of interaction.

The time window of ARH-PVH projection development coincides with the postnatal leptin surge (Ahima et al. 1998; Bouret et al. 2004b). Preliminary previous data indicated that the AP-NTS projections are already present on postnatal day 7 implying that their development takes place in the early postnatal phase or even perhaps prenatally. The AP/NTS region is involved in the short-term control of food intake, while the ARH is the main site for long-term control of body weight and energy stores. It may therefore be of importance that AP-NTS projections even develop prenatally, as neonates are confronted with a sudden change in nutritional supply at birth. The abrupt onset of ingestive behavior may require an already well-developed circuitry for the control of food intake. However, we can infer that unlike the development of ARH projections, the AP-NTS projection development does not coincide with the postnatal leptin surge that typically occurs between postnatal days 6 and 14. Like amylin (Caminos et al. 2009; Mulder et al. 1997), leptin is expressed by different fetal tissues and the placenta (Chen et al. 2000; Hoggard et al. 1997), which is compatible with the idea of a potentially prenatal trophic action of leptin in addition to its early postnatal effects.

A further interesting finding in our study with leptin-deficient mice was the apparent genotype-specific difference in the fiber density of the long AP efferents, projecting ventrolaterally. We performed semi-quantitative analysis under the fluorescence microscope, which revealed that the density of these projections also seems to be reduced in leptin-deficient mice. These projections have terminal fields in the nucleus ambiguus and the parabrachial nucleus (PBN) (Shapiro and Miselis 1985; van der Kooy and Koda 1983), but it remains to be elucidated if fibers to both projection sites were reduced. We hypothesize that fibers to the PBN may at least to some extent be affected, as the PBN plays an important role as a relay center, transmitting amylin signaling from the AP to rostral brain areas (Becskei et al. 2007).

In conclusion, the current study further characterizes the neurotrophic effect of amylin on the development of AP-NTS projections, and also provides strong evidence for a neurotrophic effect of leptin on the AP-NTS projections.

Calcitonin receptors in adult IAPP$^{-/-}$ mice appear to be increased, which is indicative of an autoregulatory mechanism adjusting receptor-ligand interactions (Huang et al. 1997; Kuwasako et al. 2000). Apart from that, there was no indication of alterations in the neuroanatomy or signal transduction in the AP/NTS region of adult IAPP$^{-/-}$ mice, although these studies require further investigation. However, we put forward the hypothesis that

abnormal development of neuronal circuits in early postnatal IAPP$^{-/-}$ mice might lead to a secondary functional or neuroanatomical imprinting with consequences for the adult individual. Which hormonal or neuronal systems are affected and whether these mechanisms only affect the control of energy balance remains to be elucidated.

Our study provides the first evidence that leptin is necessary for the development of brainstem circuits involved in the control of food intake. This important finding further extends the concept that leptin functions as a developmental factor, which is required for appropriate maturation of brain circuits involved in the maintenance of energy balance. Possible interactions of amylin and leptin during early postnatal brain development will be investigated in follow up studies of ARH and AP projections in amylin / leptin double knockout mice. For these investigations the studies conducted in the current work constitute an important starting point. As put forward by a number of recent studies (Bouret et al. 2008), perinatal processes that modulate brain development and programming of neural circuits appear to be extremely important as determining risk factors for obesity and associated disorders later in life.

5 References

Abbott CR, Monteiro M, Small CJ, Sajedi A, Smith KL, Parkinson JR, Ghatei MA, and Bloom SR. The inhibitory effects of peripheral administration of peptide YY(3-36) and glucagon-like peptide-1 on food intake are attenuated by ablation of the vagal-brainstem-hypothalamic pathway. *Brain Research* 1044: 127-131, 2005.

Abbott NJ. Evidence for bulk flow of brain interstitial fluid: significance for physiology and pathology. *Neurochemistry International* 45: 545-552, 2004.

Abbott NJ, Ronnback L, and Hansson E. Astrocyte-endothelial interactions at the blood-brain barrier. *Nature Reviews* 7: 41-53, 2006.

Ahima RS, Bjorbaek C, Osei S, and Flier JS. Regulation of neuronal and glial proteins by leptin: implications for brain development. *Endocrinology* 140: 2755-2762, 1999.

Ahima RS, and Hileman SM. Postnatal regulation of hypothalamic neuropeptide expression by leptin: implications for energy balance and body weight regulation. *Regulatory Peptides* 92: 1-7, 2000.

Ahima RS, Prabakaran D, and Flier JS. Postnatal leptin surge and regulation of circadian rhythm of leptin by feeding. Implications for energy homeostasis and neuroendocrine function. *The Journal of Clinical Investigation* 101: 1020-1027, 1998.

Anand BK, and Pillai RV. Activity of single neurons in the hypothalamic feeding centres: effect of gastric distension. *The Journal of Physiology* 192: 63-77, 1967.

Armstrong WE, Tian M, and Wong H. Electron microscopic analysis of synaptic inputs from the median preoptic nucleus and adjacent regions to the supraoptic nucleus in the rat. *The Journal of Comparative Neurology* 373: 228-239, 1996.

Asai J, Nakazato M, Miyazato M, Kangawa K, Matsuo H, and Matsukura S. Regional distribution and molecular forms of rat islet amyloid polypeptide. *Biochemical and Biophysical Research Communications* 169: 788-795, 1990.

Banks WA, Jaspan JB, Huang W, and Kastin AJ. Transport of insulin across the blood-brain barrier: saturability at euglycemic doses of insulin. *Peptides* 18: 1423-1429, 1997.

Banks WA, Kastin AJ, Huang W, Jaspan JB, and Maness LM. Leptin enters the brain by a saturable system independent of insulin. *Peptides* 17: 305-311, 1996.

Barberis C, and Tribollet E. Vasopressin and oxytocin receptors in the central nervous system. *Critical Reviews in Neurobiology* 10: 119-154, 1996.

Baskin DG, Hahn TM, and Schwartz MW. Leptin sensitive neurons in the hypothalamus. *Hormone and Metabolic Research* 31: 345-350, 1999.

Baskin DG, Wilcox BJ, Figlewicz DP, and Dorsa DM. Insulin and insulin-like growth factors in the CNS. *Trends in Neurosciences* 11: 107-111, 1988.

Batterham RL, Cowley MA, Small CJ, Herzog H, Cohen MA, Dakin CL, Wren AM, Brynes AE, Low MJ, Ghatei MA, Cone RD, and Bloom SR. Gut hormone PYY(3-36) physiologically inhibits food intake. *Nature* 418: 650-654, 2002.

Beck B, Stricker-Krongrad A, Nicolas JP, and Burlet C. Chronic and continuous intracerebroventricular infusion of neuropeptide Y in Long-Evans rats mimics the feeding behaviour of obese Zucker rats. *International Journal of Obesity and Related Metabolic Disorders* 16: 295-302, 1992.

Becskei C, Grabler V, Edwards GL, Riediger T, and Lutz TA. Lesion of the lateral parabrachial nucleus attenuates the anorectic effect of peripheral amylin and CCK. *Brain Research* 1162: 76-84, 2007.

Belgardt BF, Okamura T, and Bruning JC. Hormone and glucose signalling in POMC and AgRP neurons. *The Journal of Physiology* 587: 5305-5314, 2009.

Benoit SC, Air EL, Coolen LM, Strauss R, Jackman A, Clegg DJ, Seeley RJ, and Woods SC. The catabolic action of insulin in the brain is mediated by melanocortins. *J Neurosci* 22: 9048-9052, 2002.

Berger BD, Wise CD, and Stein L. Area postrema damage and bait shyness. *Journal of Comparative and Physiological Psychology* 82: 475-479, 1973.

Bernal J. Action of thyroid hormone in brain. *Journal of Endocrinological Investigation* 25: 268-288, 2002.

Berridge KC. Motivation concepts in behavioral neuroscience. *Physiology & Behavior* 81: 179-209, 2004.

Bhandari P, Bingham S, and Andrews PL. The neuropharmacology of loperamide-induced emesis in the ferret: the role of the area postrema, vagus, opiate and 5-HT3 receptors. *Neuropharmacology* 31: 735-742, 1992.

Billington CJ, Briggs JE, Grace M, and Levine AS. Effects of intracerebroventricular injection of neuropeptide Y on energy metabolism. *The American Journal of Physiology* 260: R321-327, 1991.

Bishop VS, Hasser EM, and Nair UC. Baroreflex control of renal nerve activity in conscious animals. *Circulation Research* 61: I76-81, 1987.

Bjorntorp P. Body fat distribution, insulin resistance, and metabolic diseases. *Nutrition* 13: 795-803, 1997.

Blevins JE, Stanley BG, and Reidelberger RD. Brain regions where cholecystokinin suppresses feeding in rats. *Brain Research* 860: 1-10, 2000.

Borison HL. Area postrema: chemoreceptor trigger zone for vomiting--is that all? *Life Sciences* 14: 1807-1817, 1974.

Borison HL, and Wang SC. Physiology and pharmacology of vomiting. *Pharmacological Reviews* 5: 193-230, 1953.

Bouret SG, Draper SJ, and Simerly RB. Formation of projection pathways from the arcuate nucleus of the hypothalamus to hypothalamic regions implicated in the neural control of feeding behavior in mice. *Journal of Neuroscience* 24: 2797-2805, 2004a.

Bouret SG, Draper SJ, and Simerly RB. Trophic action of leptin on hypothalamic neurons that regulate feeding. *Science* 304: 108-110, 2004b.

Bouret SG, Gorski JN, Patterson CM, Chen S, Levin BE, and Simerly RB. Hypothalamic neural projections are permanently disrupted in diet-induced obese rats. *Cell Metabolism* 7: 179-185, 2008.

Cai Y, and Bishop VS. Effects of arginine vasopressin and angiotensin II on area postrema neurons in rabbit brain slice preparation. *Neuroscience Letters* 190: 125-128, 1995.

Caminos JE, Bravo SB, Garces MF, Gonzalez CR, Cepeda LA, Gonzalez AC, Nogueiras R, Gallego R, Garcia-Caballero T, Cordido F, Lopez M, and Dieguez C. Vaspin and amylin are expressed in human and rat placenta and regulated by nutritional status. *Histology and Histopathology* 24: 979-990, 2009.

Carlberg M, Gundlach AL, Mercer LD, and Beart PM. Autoradiographic Localization of Cholecystokinin A and B Receptors in Rat Brain Using [125I]d-Tyr25 (Nle28,31)-CCK 25 - 33S. *The European Journal of Neuroscience* 4: 563-573, 1992.

Carpenter DO, Briggs DB, and Strominger N. Responses of neurons of canine area postrema to neurotransmitters and peptides. *Cellular and Molecular Neurobiology* 3: 113-126, 1983.

Chen H, Charlat O, Tartaglia LA, Woolf EA, Weng X, Ellis SJ, Lakey ND, Culpepper J, Moore KJ, Breitbart RE, Duyk GM, Tepper RI, and Morgenstern JP. Evidence that the diabetes gene encodes the leptin receptor: identification of a mutation in the leptin receptor gene in db/db mice. *Cell* 84: 491-495, 1996.

Chen X, Lin J, Hausman DB, Martin RJ, Dean RG, and Hausman GJ. Alterations in fetal adipose tissue leptin expression correlate with the development of adipose tissue. *Biology of the Neonate* 78: 41-47, 2000.

Chua SC, Jr., Chung WK, Wu-Peng XS, Zhang Y, Liu SM, Tartaglia L, and Leibel RL. Phenotypes of mouse diabetes and rat fatty due to mutations in the OB (leptin) receptor. *Science (New York, NY* 271: 994-996, 1996.

Clark A, Cooper GJ, Lewis CE, Morris JF, Willis AC, Reid KB, and Turner RC. Islet amyloid formed from diabetes-associated peptide may be pathogenic in type-2 diabetes. *Lancet* 2: 231-234, 1987.

Cooper GJ, Leighton B, Dimitriadis GD, Parry-Billings M, Kowalchuk JM, Howland K, Rothbard JB, Willis AC, and Reid KB. Amylin found in amyloid deposits in human type 2 diabetes mellitus may be a hormone that regulates glycogen metabolism in skeletal muscle. *Proceedings of the National Academy of Sciences of the United States of America* 85: 7763-7766, 1988.

Cooper GJ, Willis AC, Clark A, Turner RC, Sim RB, and Reid KB. Purification and characterization of a peptide from amyloid-rich pancreases of type 2 diabetic patients. *Proceedings of the National Academy of Sciences of the United States of America* 84: 8628-8632, 1987.

Cornish J, Callon KE, Bava U, Kamona SA, Cooper GJ, and Reid IR. Effects of calcitonin, amylin, and calcitonin gene-related peptide on osteoclast development. *Bone* 29: 162-168, 2001.

Cornish J, Callon KE, Cooper GJ, and Reid IR. Amylin stimulates osteoblast proliferation and increases mineralized bone volume in adult mice. *Biochemical and Biophysical Research Communications* 207: 133-139, 1995.

Dacquin R, Davey RA, Laplace C, Levasseur R, Morris HA, Goldring SR, Gebre-Medhin S, Galson DL, Zajac JD, and Karsenty G. Amylin inhibits bone resorption while the calcitonin receptor controls bone formation in vivo. *The Journal of Cell Biology* 164: 509-514, 2004.

Dallaporta M, Pecchi E, Pio J, Jean A, Horner KC, and Troadec JD. Expression of leptin receptor by glial cells of the nucleus tractus solitarius: possible involvement in energy homeostasis. *Journal of Neuroendocrinology* 21: 57-67, 2009.

Davis JD, and Campbell CS. Peripheral control of meal size in the rat. Effect of sham feeding on meal size and drinking rate. *Journal of Comparative Physiology and Psychology* 83: 379-387, 1973.

Denijn M, De Weger RA, Van Mansfeld AD, van Unnik JA, and Lips CJ. Islet amyloid polypeptide (IAPP) is synthesized in the islets of Langerhans. Detection of IAPP polypeptide and IAPP mRNA by combined in situ hybridization and immunohistochemistry in rat pancreas. *Histochemistry* 97: 33-37, 1992.

Dua A, Hennes MI, Hoffmann RG, Maas DL, Krakower GR, Sonnenberg GE, and Kissebah AH. Leptin: a significant indicator of total body fat but not of visceral fat and insulin insensitivity in African-American women. *Diabetes* 45: 1635-1637, 1996.

Edelman SV, and Caballero L. Amylin replacement therapy in patients with type 1 diabetes. *The Diabetes Educator* 32 Suppl 3: 119S-127S, 2006.

Elmquist JK, Coppari R, Balthasar N, Ichinose M, and Lowell BB. Identifying hypothalamic pathways controlling food intake, body weight, and glucose homeostasis. *The Journal of Comparative Neurology* 493: 63-71, 2005.

Ferguson AV. The area postrema: a cardiovascular control centre at the blood-brain interface? *Canadian Journal of Physiology and Pharmacology* 69: 1026-1034, 1991.

Ferguson AV, Day TA, and Renaud LP. Subfornical organ stimulation excites paraventricular neurons projecting to dorsal medulla. *The American Journal of Physiology* 247: R1088-1092, 1984.

Ferrannini E. Insulin resistance versus insulin deficiency in non-insulin-dependent diabetes mellitus: problems and prospects. *Endocrine Reviews* 19: 477-490, 1998.
Fink GD, Bruner CA, and Mangiapane ML. Area postrema is critical for angiotensin-induced hypertension in rats. *Hypertension* 9: 355-361, 1987.
Friedman JM, and Halaas JL. Leptin and the regulation of body weight in mammals. *Nature* 395: 763-770, 1998.
Fujimoto K, Machidori H, Iwakiri R, Yamamoto K, Fujisaki J, Sakata T, and Tso P. Effect of intravenous administration of apolipoprotein A-IV on patterns of feeding, drinking and ambulatory activity of rats. *Brain Research* 608: 233-237, 1993.
Geary N. Pancreatic glucagon signals postprandial satiety. *Neuroscience and Biobehavioral Reviews Rev* 14: 323-338, 1990.
Gebke E, Muller AR, Pehl U, and Gerstberger R. Astrocytes in sensory circumventricular organs of the rat brain express functional binding sites for endothelin. *Neuroscience* 97: 371-381, 2000.
Gebre-Medhin S, Mulder H, Pekny M, Westermark G, Tornell J, Westermark P, Sundler F, Ahren B, and Betsholtz C. Increased insulin secretion and glucose tolerance in mice lacking islet amyloid polypeptide (amylin). *Biochemical and Biophysical Research Communications* 250: 271-277, 1998a.
Gebre-Medhin S, Mulder H, Zhang Y, Sundler F, and Betsholtz C. Reduced nociceptive behavior in islet amyloid polypeptide (amylin) knockout mice. *Brain Research* 63: 180-183, 1998b.
Gedulin BR, Jodka CM, Herrmann K, and Young AA. Role of endogenous amylin in glucagon secretion and gastric emptying in rats demonstrated with the selective antagonist, AC187. *Regulatory Peptides* 137: 121-127, 2006.
Gedulin BR, Rink TJ, and Young AA. Dose-response for glucagonostatic effect of amylin in rats. *Metabolism: Clinical and Experimental* 46: 67-70, 1997.
Gedulin BR, and Young AA. Hypoglycemia overrides amylin-mediated regulation of gastric emptying in rats. *Diabetes* 47: 93-97, 1998.
Gibbs J, Young RC, and Smith GP. Cholecystokinin decreases food intake in rats. *Journal of Comparative Physiology and Psychology* 84: 488-495, 1973.
Gilbey SG, Ghatei MA, Bretherton-Watt D, Zaidi M, Jones PM, Perera T, Beacham J, Girgis S, and Bloom SR. Islet amyloid polypeptide: production by an osteoblast cell line and possible role as a paracrine regulator of osteoclast function in man. *Clinical Science (Lond)* 81: 803-808, 1991.
Goke R, Larsen PJ, Mikkelsen JD, and Sheikh SP. Distribution of GLP-1 binding sites in the rat brain: evidence that exendin-4 is a ligand of brain GLP-1 binding sites. *The European Journal of Neuroscience* 7: 2294-2300, 1995.
Gropp E, Shanabrough M, Borok E, Xu AW, Janoschek R, Buch T, Plum L, Balthasar N, Hampel B, Waisman A, Barsh GS, Horvath TL, and Bruning JC. Agouti-related peptide-expressing neurons are mandatory for feeding. *Nature Neuroscience* 8: 1289-1291, 2005.
Gross PM. Circumventricular organ capillaries. *Progress in Brain Research* 91: 219-233, 1992.
Guidobono F, Coluzzi M, Pagani F, Pecile A, and Netti C. Amylin given by central and peripheral routes inhibits acid gastric secretion. *Peptides* 15: 699-702, 1994.
Gutman MB, Ciriello J, and Mogenson GJ. Effects of plasma angiotensin II and hypernatremia on subfornical organ neurons. *The American Journal of Physiology* 254: R746-754, 1988.
Halaas JL, Gajiwala KS, Maffei M, Cohen SL, Chait BT, Rabinowitz D, Lallone RL, Burley SK, and Friedman JM. Weight-reducing effects of the plasma protein encoded by the obese gene. *Science (New York, NY* 269: 543-546, 1995.

Harris PJ, Cooper ME, Hiranyachattada S, Berka JL, Kelly DJ, Nobes M, and Wookey PJ. Amylin stimulates proximal tubular sodium transport and cell proliferation in the rat kidney. *The American Journal of Physiology* 272: F13-21, 1997.

Havel PJ. Mechanisms regulating leptin production: implications for control of energy balance. *American Journal of Clinical Nutrition* 70: 305-306, 1999.

Hayden MR, and Tyagi SC. "A" is for amylin and amyloid in type 2 diabetes mellitus. *Journal of the Pancreas* 2: 124-139, 2001.

Heptulla RA, Rodriguez LM, Bomgaars L, and Haymond MW. The role of amylin and glucagon in the dampening of glycemic excursions in children with type 1 diabetes. *Diabetes* 54: 1100-1107, 2005.

Hermann GE, and Rogers RC. Convergence of vagal and gustatory afferent input within the parabrachial nucleus of the rat. *Journal of the Autonomic Nervous System* 13: 1-17, 1985.

Hoffman GE, Smith MS, and Verbalis JG. c-Fos and related immediate early gene products as markers of activity in neuroendocrine systems. *Frontiers in Neuroendocrinology* 14: 173-213, 1993.

Hoggard N, Hunter L, Duncan JS, Williams LM, Trayhurn P, and Mercer JG. Leptin and leptin receptor mRNA and protein expression in the murine fetus and placenta. *Proceedings of the National Academy of Sciences of the United States of America* 94: 11073-11078, 1997.

Honig MG, and Hume RI. Dil and diO: versatile fluorescent dyes for neuronal labelling and pathway tracing. *Trends in Neurosciences* 12: 333-335, 340-331, 1989.

Huang XF, Lin S, and Zhang R. Upregulation of leptin receptor mRNA expression in obese mouse brain. *Neuroreport* 8: 1035-1038, 1997.

Hummel KP, Dickie MM, and Coleman DL. Diabetes, a new mutation in the mouse. *Science (New York, NY* 153: 1127-1128, 1966.

Hwa JJ, Witten MB, Williams P, Ghibaudi L, Gao J, Salisbury BG, Mullins D, Hamud F, Strader CD, and Parker EM. Activation of the NPY Y5 receptor regulates both feeding and energy expenditure. *The American Journal of Physiology* 277: R1428-1434, 1999.

Hyde TM, and Miselis RR. Effects of area postrema/caudal medial nucleus of solitary tract lesions on food intake and body weight. *The American Journal of Physiology* 244: R577-587, 1983.

Hyde TM, and Peroutka SJ. Distribution of cholecystokinin receptors in the dorsal vagal complex and other selected nuclei in the human medulla. *Brain Research* 495: 198-202, 1989.

Ingalls AM, Dickie MM, and Snell GD. Obese, a new mutation in the house mouse. *The Journal of Heredity* 41: 317-318, 1950.

Jamal H, Suda K, Bretherton-Watt D, Ghatei MA, and Bloom SR. Molecular form of islet amyloid polypeptide (amylin) released from isolated rat islets of Langerhans. *Pancreas* 8: 261-266, 1993.

Johnson AK, and Gross PM. Sensory circumventricular organs and brain homeostatic pathways. *FASEB Journal* 7: 678-686, 1993.

Johnson KH, O'Brien TD, Hayden DW, Jordan K, Ghobrial HK, Mahoney WC, and Westermark P. Immunolocalization of islet amyloid polypeptide (IAPP) in pancreatic beta cells by means of peroxidase-antiperoxidase (PAP) and protein A-gold techniques. *The American Journal of Pathology* 130: 1-8, 1988.

Jovanovic-Micic D, Strbac M, Krstic SK, Japundzic N, Samardzic R, and Beleslin DB. Ablation of the area postrema and emesis. *Metabolic Brain Disease* 4: 55-60, 1989.

Kalia M, and Sullivan JM. Brainstem projections of sensory and motor components of the vagus nerve in the rat. *The Journal of Comparative Neurology* 211: 248-265, 1982.

Kalra SP, Dube MG, Pu S, Xu B, Horvath TL, and Kalra PS. Interacting appetite-regulating pathways in the hypothalamic regulation of body weight. *Endocrine Reviews* 20: 68-100, 1999.

Karlsson E, and Sandler S. Islet amyloid polypeptide promotes beta-cell proliferation in neonatal rat pancreatic islets. *Diabetologia* 44: 1015-1018, 2001.
Kolterman OG, Gottlieb A, Moyses C, and Colburn W. Reduction of postprandial hyperglycemia in subjects with IDDM by intravenous infusion of AC137, a human amylin analogue. *Diabetes Care* 18: 1179-1182, 1995.
Kong MF, King P, Macdonald IA, Stubbs TA, Perkins AC, Blackshaw PE, Moyses C, and Tattersall RB. Infusion of pramlintide, a human amylin analogue, delays gastric emptying in men with IDDM. *Diabetologia* 40: 82-88, 1997.
Kosten T, and Contreras RJ. Deficits in conditioned heart rate and taste aversion in area postrema-lesioned rats. *Behavioural Brain Research* 35: 9-21, 1989.
Krisch B. Somatostatin-binding sites on structures of circumventricular organs. *Progress in Brain Research* 91: 247-250, 1992.
Krisch B, Leonhardt H, and Buchheim W. The functional and structural border between the CSF- and blood-milieu in the circumventricular organs (organum vasculosum laminae terminalis, subfornical organ, area postrema) of the rat. *Cell and Tissue Research* 195: 485-497, 1978.
Kuwasako K, Shimekake Y, Masuda M, Nakahara K, Yoshida T, Kitaura M, Kitamura K, Eto T, and Sakata T. Visualization of the calcitonin receptor-like receptor and its receptor activity-modifying proteins during internalization and recycling. *The Journal of Biological Chemistry* 275: 29602-29609, 2000.
Ladenheim EE, Wirth KE, and Moran TH. Receptor subtype mediation of feeding suppression by bombesin-like peptides. *Pharmacology Biochemistry and Behavior* 54: 705-711, 1996.
Lanca AJ, and van der Kooy D. A serotonin-containing pathway from the area postrema to the parabrachial nucleus in the rat. *Neuroscience* 14: 1117-1126, 1985.
Lind RW. Angiotensin and the lamina terminalis: illustrations of a complex unity. *Clinical and Experimental Hypertension* 10 Suppl 1: 79-105, 1988.
Lind RW, Van Hoesen GW, and Johnson AK. An HRP study of the connections of the subfornical organ of the rat. *The Journal of Comparative Neurology* 210: 265-277, 1982.
Lotter EC, Krinsky R, McKay JM, Treneer CM, Porter D, Jr., and Woods SC. Somatostatin decreases food intake of rats and baboons. *Journal of Comparative Physiology and Psychology* 95: 278-287, 1981.
Lowes VL, Sun K, Li Z, and Ferguson AV. Vasopressin actions on area postrema neurons in vitro. *The American Journal of Physiology* 269: R463-468, 1995.
Luiten PG, ter Horst GJ, and Steffens AB. The hypothalamus, intrinsic connections and outflow pathways to the endocrine system in relation to the control of feeding and metabolism. *Progress in Neurobiology* 28: 1-54, 1987.
Luquet S, and Magnan C. The central nervous system at the core of the regulation of energy homeostasis. *Frontiers of Bioscience (Schol Ed)* 1: 448-465, 2009.
Luquet S, Perez FA, Hnasko TS, and Palmiter RD. NPY/AgRP neurons are essential for feeding in adult mice but can be ablated in neonates. *Science (New York, NY* 310: 683-685, 2005.
Lutz TA. Amylinergic control of food intake. *Physiology & Behavior* 89: 465-471, 2006.
Lutz TA, Del Prete E, and Scharrer E. Reduction of food intake in rats by intraperitoneal injection of low doses of amylin. *Physiology & Behavior* 55: 891-895, 1994.
Lutz TA, Del Prete E, and Scharrer E. Subdiaphragmatic vagotomy does not influence the anorectic effect of amylin. *Peptides* 16: 457-462, 1995a.
Lutz TA, Geary N, Szabady MM, Del Prete E, and Scharrer E. Amylin decreases meal size in rats. *Physiology & Behavior* 58: 1197-1202, 1995b.
Lutz TA, Mollet A, Rushing PA, Riediger T, and Scharrer E. The anorectic effect of a chronic peripheral infusion of amylin is abolished in area postrema/nucleus of the solitary

tract (AP/NTS) lesioned rats. *International Journal of Obesity and Related Metabolic Disorders* 25: 1005-1011, 2001.
Lutz TA, Senn M, Althaus J, Del Prete E, Ehrensperger F, and Scharrer E. Lesion of the area postrema/nucleus of the solitary tract (AP/NTS) attenuates the anorectic effects of amylin and calcitonin gene-related peptide (CGRP) in rats. *Peptides* 19: 309-317, 1998.
Madeira MD, and Lieberman AR. Sexual dimorphism in the mammalian limbic system. *Progress in Neurobiology* 45: 275-333, 1995.
Maffei M, Halaas J, Ravussin E, Pratley RE, Lee GH, Zhang Y, Fei H, Kim S, Lallone R, Ranganathan S, and et al. Leptin levels in human and rodent: measurement of plasma leptin and ob RNA in obese and weight-reduced subjects. *Nature Medicine* 1: 1155-1161, 1995.
Mangurian LP, Jurjus AR, and Walsh RJ. Prolactin receptor localization to the area postrema. *Brain Research* 836: 218-220, 1999.
Matson CA, Wiater MF, Kuijper JL, and Weigle DS. Synergy between leptin and cholecystokinin (CCK) to control daily caloric intake. *Peptides* 18: 1275-1278, 1997.
McEwen BS, De Kloet ER, and Rostene W. Adrenal steroid receptors and actions in the nervous system. *Physiological Reviews* 66: 1121-1188, 1986.
McKellar S, and Loewy AD. Organization of some brain stem afferents to the paraventricular nucleus of the hypothalamus in the rat. *Brain Research* 217: 351-357, 1981.
Mendelsohn FA, Allen AM, Chai SY, Sexton PM, and Figdor R. Overlapping distributions of receptors for atrial natriuretic peptide and angiotensin II visualized by in vitro autoradiography: morphological basis of physiological antagonism. *Canadian Journal of Physiology and Pharmacology* 65: 1517-1521, 1987.
Mercer JG, Hoggard N, Williams LM, Lawrence CB, Hannah LT, and Trayhurn P. Localization of leptin receptor mRNA and the long form splice variant (Ob-Rb) in mouse hypothalamus and adjacent brain regions by in situ hybridization. *FEBS Letters* 387: 113-116, 1996.
Miller AD, and Nonaka S. Mechanisms of vomiting induced by serotonin-3 receptor agonists in the cat: effect of vagotomy, splanchnicectomy or area postrema lesion. *The Journal of Pharmacology and Experimental Therapeutics* 260: 509-517, 1992.
Minor RK, Chang JW, and de Cabo R. Hungry for life: How the arcuate nucleus and neuropeptide Y may play a critical role in mediating the benefits of calorie restriction. *Molecular and Cellular Endocrinology* 299: 79-88, 2009.
Miselis RR. The subfornical organ's neural connections and their role in water balance. *Peptides* 3: 501-502, 1982.
Miselis RR, Shapiro RE, and Hand PJ. Subfornical organ efferents to neural systems for control of body water. *Science (New York, NY* 205: 1022-1025, 1979.
Mistry AM, Swick A, and Romsos DR. Leptin alters metabolic rates before acquisition of its anorectic effect in developing neonatal mice. *The American Journal of Physiology* 277: R742-747, 1999.
Mitsukawa T, Takemura J, Asai J, Nakazato M, Kangawa K, Matsuo H, and Matsukura S. Islet amyloid polypeptide response to glucose, insulin, and somatostatin analogue administration. *Diabetes* 39: 639-642, 1990.
Molavi B, Rasouli N, and Kern PA. The prevention and treatment of metabolic syndrome and high-risk obesity. *Current Opinion in Cardiology* 21: 479-485, 2006.
Mollet A, Gilg S, Riediger T, and Lutz TA. Infusion of the amylin antagonist AC 187 into the area postrema increases food intake in rats. *Physiology & Behavior* 81: 149-155, 2004.
Moran TH, Baldessarini AR, Salorio CF, Lowery T, and Schwartz GJ. Vagal afferent and efferent contributions to the inhibition of food intake by cholecystokinin. *American Journal of Physiology* 272: R1245-1251, 1997.

Moriyasu M, Lee YL, Lee KY, Chang TM, and Chey WY. Effect of digested protein on pancreatic exocrine secretion and gut hormone release in the dog. *Pancreas* 9: 129-133, 1994.
Morley JE, Suarez MD, Mattamal M, and Flood JF. Amylin and food intake in mice: effects on motivation to eat and mechanism of action. *Pharmacology, Biochemistry and Behavior* 56: 123-129, 1997.
Mosselman S, Hoppener JW, Zandberg J, van Mansfeld AD, Geurts van Kessel AH, Lips CJ, and Jansz HS. Islet amyloid polypeptide: identification and chromosomal localization of the human gene. *FEBS Letters* 239: 227-232, 1988.
Muff R, Buhlmann N, Fischer JA, and Born W. An amylin receptor is revealed following co-transfection of a calcitonin receptor with receptor activity modifying proteins-1 or -3. *Endocrinology* 140: 2924-2927, 1999.
Mulder H, Ekelund M, Ekblad E, and Sundler F. Islet amyloid polypeptide in the gut and pancreas: localization, ontogeny and gut motility effects. *Peptides* 18: 771-783, 1997.
Mulder H, Leckstrom A, Uddman R, Ekblad E, Westermark P, and Sundler F. Islet amyloid polypeptide (amylin) is expressed in sensory neurons. *Journal of Neuroscience* 15: 7625-7632, 1995.
Nakajima T, Yashima Y, and Nakamura K. Quantitative autoradiographic localization of neuropeptide Y receptors in the rat lower brainstem. *Brain Research* 380: 144-150, 1986.
Naslund E, Barkeling B, King N, Gutniak M, Blundell JE, Holst JJ, Rossner S, and Hellstrom PM. Energy intake and appetite are suppressed by glucagon-like peptide-1 (GLP-1) in obese men. *International Journal of Obesity and Related Metabolic Disorders* 23: 304-311, 1999.
Ogawa A, Harris V, McCorkle SK, Unger RH, and Luskey KL. Amylin secretion from the rat pancreas and its selective loss after streptozotocin treatment. *The Journal of Clinical Investigation* 85: 973-976, 1990.
Okada S, York DA, Bray GA, and Erlanson-Albertsson C. Enterostatin (Val-Pro-Asp-Pro-Arg), the activation peptide of procolipase, selectively reduces fat intake. *Physiology & Behavior* 49: 1185-1189, 1991.
Oosterwijk C, Hoppener JW, van Hulst KL, and Lips CJ. Pancreatic islet amyloid formation in patients with noninsulin-dependent diabetes mellitus. Implication for therapeutic strategy. *International Journal of Pancreatology* 18: 7-14, 1995.
Oppenheimer JH, Schwartz HL, Mariash CN, Kinlaw WB, Wong NC, and Freake HC. Advances in our understanding of thyroid hormone action at the cellular level. *Endocrine Reviews* 8: 288-308, 1987.
Palkovits M, and Zaborszky L. Neuroanatomy of central cardiovascular control. Nucleus tractus solitarii: afferent and efferent neuronal connections in relation to the baroreceptor reflex arc. *Progress in Brain Research* 47: 9-34, 1977.
Papas S, and Ferguson AV. Electrophysiological characterization of reciprocal connections between the parabrachial nucleus and the area postrema in the rat. *Brain Research Bulletin* 24: 577-582, 1990.
Pelleymounter MA, Cullen MJ, Baker MB, Hecht R, Winters D, Boone T, and Collins F. Effects of the obese gene product on body weight regulation in ob/ob mice. *Science (New York, NY* 269: 540-543, 1995.
Pinto S, Roseberry AG, Liu H, Diano S, Shanabrough M, Cai X, Friedman JM, and Horvath TL. Rapid rewiring of arcuate nucleus feeding circuits by leptin. *Science (New York, NY* 304: 110-115, 2004.
Polonsky KS, Given BD, and Van Cauter E. Twenty-four-hour profiles and pulsatile patterns of insulin secretion in normal and obese subjects. *J Clin Invest* 81: 442-448, 1988.
Popkin BM, and Doak CM. The obesity epidemic is a worldwide phenomenon. *Nutrition Reviews* 56: 106-114, 1998.

Rabin BM, and Hunt WA. Interaction of haloperidol and area postrema lesions in the disruption of amphetamine-induced conditioned taste aversion learning in rats. *Pharmacology, Biochemistry and Behavior* 33: 847-851, 1989.
Reidelberger RD, Haver AC, Arnelo U, Smith DD, Schaffert CS, and Permert J. Amylin receptor blockade stimulates food intake in rats. *American Journal of Physiology* 287: R568-574, 2004.
Ricardo JA, and Koh ET. Anatomical evidence of direct projections from the nucleus of the solitary tract to the hypothalamus, amygdala, and other forebrain structures in the rat. *Brain Research* 153: 1-26, 1978.
Riediger T, Schmid HA, Lutz T, and Simon E. Amylin potently activates AP neurons possibly via formation of the excitatory second messenger cGMP. *American Journal of Physiology* 281: R1833-1843, 2001.
Riediger T, Schmid HA, Young AA, and Simon E. Pharmacological characterisation of amylin-related peptides activating subfornical organ neurones. *Brain Research* 837: 161-168, 1999.
Riediger T, Zuend D, Becskei C, and Lutz TA. The anorectic hormone amylin contributes to feeding-related changes of neuronal activity in key structures of the gut-brain axis. *American Journal of Physiology* 286: R114-122, 2004.
Riedy CA, Chavez M, Figlewicz DP, and Woods SC. Central insulin enhances sensitivity to cholecystokinin. *Physiology & Behavior* 58: 755-760, 1995.
Rinaman L, Card JP, Schwaber JS, and Miselis RR. Ultrastructural demonstration of a gastric monosynaptic vagal circuit in the nucleus of the solitary tract in rat. *Journal of Neuroscience* 9: 1985-1996, 1989.
Ritter S, McGlone JJ, and Kelley KW. Absence of lithium-induced taste aversion after area postrema lesion. *Brain Research* 201: 501-506, 1980.
Rowland NE, Crews EC, and Gentry RM. Comparison of Fos induced in rat brain by GLP-1 and amylin. *Regulatory Peptides* 71: 171-174, 1997.
Sakumoto T, Tohyama M, Satoh K, Kimoto Y, Kinugasa T, Tanizawa O, Kurachi K, and Shimizu N. Afferent fiber connections from lower brain stem to hypothalamus studied by the horseradish peroxidase method with special reference to noradrenaline innervation. *Experimental Brain Research Experimentelle Hirnforschung* 31: 81-94, 1978.
Schmid HA, Rauch M, and Koch J. Effect of calcitonin on the activity of ANG II-responsive neurons in the rat subfornical organ. *The American Journal of Physiology* 274: R1646-1652, 1998.
Schmitz O, Brock B, and Rungby J. Amylin agonists: a novel approach in the treatment of diabetes. *Diabetes* 53 Suppl 3: S233-238, 2004.
Sexton PM, Paxinos G, Kenney MA, Wookey PJ, and Beaumont K. In vitro autoradiographic localization of amylin binding sites in rat brain. *Neuroscience* 62: 553-567, 1994.
Shapiro RE, and Miselis RR. The central neural connections of the area postrema of the rat. *The Journal of Comparative Neurology* 234: 344-364, 1985.
Shargill NS, Tsujii S, Bray GA, and Erlanson-Albertsson C. Enterostatin suppresses food intake following injection into the third ventricle of rats. *Brain Research* 544: 137-140, 1991.
Sharp FR, Sagar SM, Hicks K, Lowenstein D, and Hisanaga K. c-fos mRNA, Fos, and Fos-related antigen induction by hypertonic saline and stress. *Journal of Neuroscience* 11: 2321-2331, 1991.
Simerly RB. Wired for reproduction: organization and development of sexually dimorphic circuits in the mammalian forebrain. *Annual Review of Neuroscience* 25: 507-536, 2002.
Skofitsch G, Wimalawansa SJ, Jacobowitz DM, and Gubisch W. Comparative immunohistochemical distribution of amylin-like and calcitonin gene related peptide like

immunoreactivity in the rat central nervous system. *Canadian Journal of Physiology and Pharmacology* 73: 945-956, 1995.
Sofroniew MV. Direct reciprocal connections between the bed nucleus of the stria terminalis and dorsomedial medulla oblongata: evidence from immunohistochemical detection of tracer proteins. *The Journal of Comparative Neurology* 213: 399-405, 1983.
Stanley BG, Kyrkouli SE, Lampert S, and Leibowitz SF. Neuropeptide Y chronically injected into the hypothalamus: a powerful neurochemical inducer of hyperphagia and obesity. *Peptides* 7: 1189-1192, 1986.
Stein LJ, and Woods SC. Gastrin releasing peptide reduces meal size in rats. *Peptides* 3: 833-835, 1982.
Steppan CM, and Swick AG. A role for leptin in brain development. *Biochemical and Biophysical Research Communications* 256: 600-602, 1999.
Tartaglia LA. The leptin receptor. *Journal of Biological Chemistry* 272: 6093-6096, 1997.
Ter Horst GJ, de Boer P, Luiten PG, and van Willigen JD. Ascending projections from the solitary tract nucleus to the hypothalamus. A Phaseolus vulgaris lectin tracing study in the rat. *Neuroscience* 31: 785-797, 1989.
Trinh T, van Dumont Y, and Quirion R. High levels of specific neuropeptide Y/pancreatic polypeptide receptors in the rat hypothalamus and brainstem. *European Journal of Pharmacology* 318: R1-3, 1996.
Turek VF, Trevaskis JL, Levin BE, Dunn-Meynell AA, Irani B, Gu G, Wittmer C, Griffin PS, Vu C, Parkes DG, and Roth JD. Mechanisms of amylin/leptin synergy in rodent models. *Endocrinology* 151: 143-152.
Undesser KP, Hasser EM, Haywood JR, Johnson AK, and Bishop VS. Interactions of vasopressin with the area postrema in arterial baroreflex function in conscious rabbits. *Circulation Research* 56: 410-417, 1985.
Unger RH, and Orci L. The role of glucagon in the endogenous hyperglycemia of diabetes mellitus. *Annual Review of Medicine* 28: 119-130, 1977.
van der Kooy D, and Koda LY. Organization of the projections of a circumventricular organ: the area postrema in the rat. *The Journal of Comparative Neurology* 219: 328-338, 1983.
van Giersbergen PL, Palkovits M, and De Jong W. Involvement of neurotransmitters in the nucleus tractus solitarii in cardiovascular regulation. *Physiological Reviews* 72: 789-824, 1992.
Vigier D, and Rouviere A. Afferent and efferent connections of the area postrema demonstrated by the horseradish peroxidase method. *Archives Italiennes de Biologie* 117: 325-339, 1979.
Wang J, Irnaten M, Neff RA, Venkatesan P, Evans C, Loewy AD, Mettenleiter TC, and Mendelowitz D. Synaptic and neurotransmitter activation of cardiac vagal neurons in the nucleus ambiguus. *Annals of the New York Academy of Sciences* 940: 237-246, 2001.
Weindl A, Bufler J, Winkler B, Arzberger T, and Hatt H. Neurotransmitters and receptors in the subfornical organ. Immunohistochemical and electrophysiological evidence. *Progress in Brain Research* 91: 261-269, 1992.
Weiss ML, and Hatton GI. Collateral input to the paraventricular and supraoptic nuclei in rat. I. Afferents from the subfornical organ and the anteroventral third ventricle region. *Brain Research Bulletin* 24: 231-238, 1990.
Westermark P, Wernstedt C, Wilander E, Hayden DW, O'Brien TD, and Johnson KH. Amyloid fibrils in human insulinoma and islets of Langerhans of the diabetic cat are derived from a neuropeptide-like protein also present in normal islet cells. *Proceedings of the National Academy of Sciences of the United States of America* 84: 3881-3885, 1987.

Westermark P, Wernstedt C, Wilander E, and Sletten K. A novel peptide in the calcitonin gene related peptide family as an amyloid fibril protein in the endocrine pancreas. *Biochemical and Biophysical Research Communications* 140: 827-831, 1986.
Wikberg JE, Mutulis F, Mutule I, Veiksina S, Lapinsh M, Petrovska R, and Prusis P. Melanocortin receptors: ligands and proteochemometrics modeling. *Annals of the New York Academy of Sciences* 994: 21-26, 2003.
Wimalawansa SJ. Amylin, calcitonin gene-related peptide, calcitonin, and adrenomedullin: a peptide superfamily. *Critical Reviews in Neurobiology* 11: 167-239, 1997.
Woods SC, Benoit SC, Clegg DJ, and Seeley RJ. Clinical endocrinology and metabolism. Regulation of energy homeostasis by peripheral signals. *Best Practice and Research: Clinical Endocrinology & Metabolism,* 18: 497-515, 2004.
Woods SC, Schwartz MW, Baskin DG, and Seeley RJ. Food intake and the regulation of body weight. *Annual Review of Psychology* 51: 255-277, 2000.
Wookey PJ, Tikellis C, Nobes M, Casley D, Cooper ME, and Darby IA. Amylin as a growth factor during fetal and postnatal development of the rat kidney. *Kidney International* 53: 25-30, 1998.
Yang B, and Ferguson AV. Orexin-A depolarizes dissociated rat area postrema neurons through activation of a nonselective cationic conductance. *Journal of Neuroscience* 22: 6303-6308, 2002.
Yaswen L, Diehl N, Brennan MB, and Hochgeschwender U. Obesity in the mouse model of pro-opiomelanocortin deficiency responds to peripheral melanocortin. *Nature Medicine* 5: 1066-1070, 1999.
Young A. Role of amylin in nutrient intake - animal studies. *Diabetic Medicine* 14 Suppl 2: S14-18, 1997.
Young AA, Gedulin B, Vine W, Percy A, and Rink TJ. Gastric emptying is accelerated in diabetic BB rats and is slowed by subcutaneous injections of amylin. *Diabetologia* 38: 642-648, 1995.
Zarjevski N, Cusin I, Vettor R, Rohner-Jeanrenaud F, and Jeanrenaud B. Chronic intracerebroventricular neuropeptide-Y administration to normal rats mimics hormonal and metabolic changes of obesity. *Endocrinology* 133: 1753-1758, 1993.
Zhang Y, Proenca R, Maffei M, Barone M, Leopold L, and Friedman JM. Positional cloning of the mouse obese gene and its human homologue. *Nature* 372: 425-432, 1994.
Ziotopoulou M, Mantzoros CS, Hileman SM, and Flier JS. Differential expression of hypothalamic neuropeptides in the early phase of diet-induced obesity in mice. *American Journal of Physiology* 279: E838-845, 2000.
Zumpe ET, Tilakaratne N, Fraser NJ, Christopoulos G, Foord SM, and Sexton PM. Multiple ramp domains are required for generation of amylin receptor phenotype from the calcitonin receptor gene product. *Biochemical and Biophysical Research Communications* 267: 368-372, 2000.

6 Acknowledgement

I would like to thank everyone who supported me over the past half year and helped me conduct the experiments and write my thesis.

First of all, I want to express my gratitude to my supervisor PD Dr. Thomas Riediger for teaching me the methods and for his support during my experiments and especially during the last month.

Next, I would like to thank Prof. Dr. Thomas A. Lutz for having me in his group and for giving me the opportunity to gather first experience in research.

Many thanks to Prof. Dr. Adrian Hehl, Institute of Parasitology, University of Zurich and to Elisabeth Schraner, EM Lab Institutes of Vet. Anatomy and Virology, University of Zurich, for all the help with the confocal laser microscope; to Michael Koss, Institute of Animal Sciences, ETH Zurich, for his helpful advice on the PCR.

Furthermore, I want to thank Prof. Dr. S. Bouret and S. Steculorum for the collaboration in the *ob/ob* project.

Many thanks go to Caro, Catarina, Christian, Christina, Dani, Daniela, Daria, Karoline, Kerstin, Manu, Melania, Mélanie, Nadine and Sarah for all the help and motivation, and especially for the great atmosphere. I really appreciated working with you! A special thank you to Andreas for his help when it was most needed.

Finally, I want to thank my parents, my brother, all my friends and my boyfriend for all the support, motivation and understanding not only during my work on the thesis, but during everything it took to get to this point.

Curriculum Vitae

Personal Details

Name	Kathrin Abegg
Address	Fachstrasse 14 8942 Oberrieden Switzerland
Telephone	078 726 81 06
E-mail	kathrin.abegg@uzh.ch
Date of birth	February 14th 1986

Education

1992 – 1998	Primary school, Oberrieden
1998 – 2004	Secondary School, Gymnasium Kantonsschule Freudenberg, Zurich
2005 – 2010	Study of veterinary medicine, University of Zurich (In-depth study biomedical research)
Mar 2009	Start with thesis project, parallel to the study, entitled "Involvement of amylin and leptin in early developmental programming of brain pathways controlling energy balance and body weight", under supervision of PD Dr. Th. Riediger (Institute of Veterinary Physiology)

Work experience

Nov 2004 – Jan 2005	Work placement at the veterinary clinic of Zurich (small animal internal medicine)
Jun 2005 – 2009	Part-time employment at the veterinary clinic of Zurich (assistance in weekend and emergency duty)